HHS Public Access

Author manuscript

Cell. Author manuscript; available in PMC 2024 June 22.

Published in final edited form as:

Cell. 2023 June 22; 186(13): 2839–2852.e21. doi:10.1016/j.cell.2023.05.037.

Strain dropouts reveal interactions that govern the metabolic output of the gut microbiome

Min Wang[1,2,3,9], **Lucas J. Osborn**[4,5], **Sunit Jain**[3,6], **Xiandong Meng**[1,2,3], **Allison Weakley**[3,6], **Jia Yan**[6], **William J. Massey**[4,5], **Venkateshwari Varadharajan**[4,5], **Anthony Horak**[4,5], **Rakhee Banerjee**[4,5], **Daniela S. Allende**[7], **Ricky E. Chan**[8], **Adeline M. Hajjar**[4,5], **Zeneng Wang**[4,5], **Alejandra Dimas**[1,2,3], **Aishan Zhao**[1,2,3], **Kazuki Nagashima**[1,2,3], **Alice G. Cheng**[1,2,3], **Steven Higginbottom**[2,3], **Stanley Hazen**[4,5], **J. Mark Brown**[4,5], **Michael A. Fischbach**[1,2,3,6,†]

[1]Department of Bioengineering, Stanford University, Stanford, CA 94305, USA

[2]Department of Microbiology and Immunology, Stanford University School of Medicine, Stanford University, Stanford, CA 94305, USA

[3]ChEM-H Institute, Stanford University, Stanford, CA 94305, USA

[4]Department of Cardiovascular and Metabolic Sciences, Lerner Research Institute Cleveland Clinic, Cleveland, OH 44195, USA

[5]Center for Microbiome and Human Health, Lerner Research Institute, Cleveland Clinic, Cleveland, OH 44195, USA

[6]Chan Zuckerberg Biohub, San Francisco, CA 94158, USA

[7]Department of Anatomical Pathology, Cleveland Clinic, Cleveland, OH 44195, USA

[8]Institute for Computational Biology, Case Western Reserve University, Cleveland, OH 44106, USA

[9]Present address: Department of Pharmacokinetics and Drug Metabolism, Amgen Inc., South San Francisco, CA 94080, USA

Abstract

[†]Lead contact: fischbach@fischbachgroup.org.

AUTHOR CONTRIBUTIONS

Conceptualization: M.W., J.M.B., and M.A.F.; Methodology and investigation: M.W., L.J.O., S.J., X.M., A.W., J.Y., W.J.M., V.V., A.H., R.B., D.S.A., R.E.C., A.M.H., Z.W., A.D., A.Z., K.N., A.G.C., and S.H.; Visualization: M.W. and M.A.F.; Supervision: J.M.B. and M.A.F.; Writing: M.W. and M.A.F.; All authors discussed the results, commented on the manuscript, and/or added to the manuscript.

DECLARATION OF INTERESTS

Stanford University and the Chan Zuckerberg Biohub have patents pending for microbiome technologies on which the authors are co-inventors. M.A.F. is a co-founder and director of Federation Bio and Kelonia, a co-founder of Revolution Medicines, an Innovation Partner at the Column Group, and a member of the scientific advisory board of NGM Bio. All of the other authors have no competing interests.

The gut microbiome is complex, raising questions about the role of individual strains in the community. Here, we address this question by constructing variants of a complex defined community in which we eliminate strains that occupy the bile acid 7α-dehydroxylation niche. Omitting *Clostridium scindens* (*Cs*) and *Clostridium hylemonae* (*Ch*) eliminates secondary bile acid production and reshapes the community in a highly specific manner: eight strains change in relative abundance by >100-fold. In single-strain dropout communities, *Cs* and *Ch* reach the same relative abundance and dehydroxylate bile acids to a similar extent. However, *Clostridium sporogenes* increases >1000-fold in the Δ*Cs* but not Δ*Ch* dropout, reshaping the pool of microbiome-derived phenylalanine metabolites. Thus, strains that are functionally redundant within a niche can have widely varying impacts outside the niche, and a strain swap can ripple through the community in an unpredictable manner, resulting in a large impact on an unrelated community-level phenotype.

Graphical Abstract

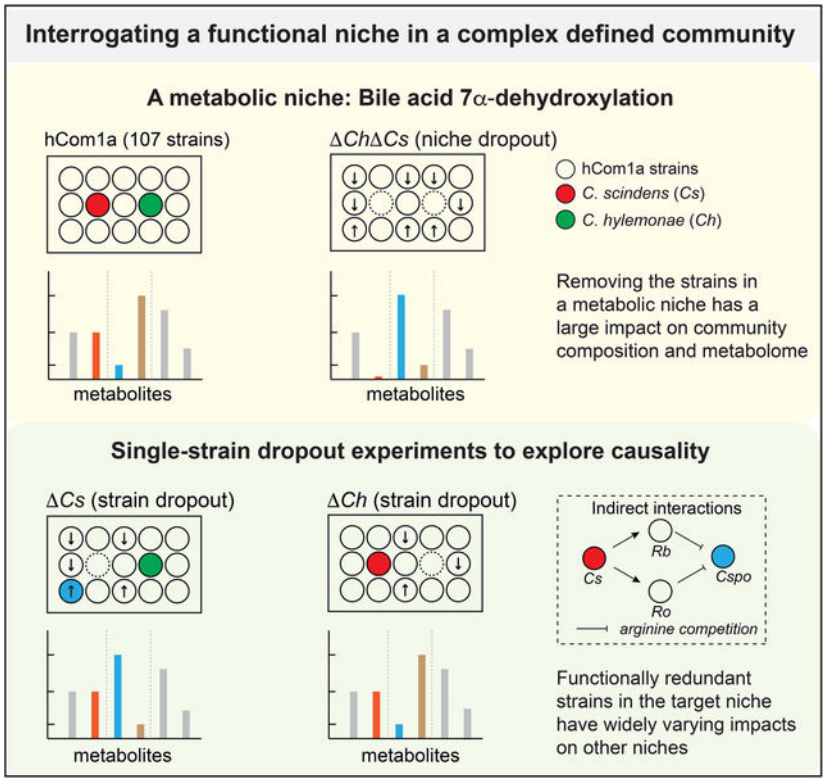

IN BRIEF

Construction of variants of a complex defined microbial community reveals that strains that are functionally redundant within a niche can have widely varying impacts outside the niche.

INTRODUCTION

A typical gut microbiome consists of several hundred bacterial strains that span at least six orders of magnitude in relative abundance. Determining the contribution of individual strains

to community ecology and host physiology is a daunting challenge. A variety of studies have characterized the functional properties of bacterial strains from the gut microbiome[1–10]. However, in vivo demonstrations of function typically involve mice colonized by one species or a small community; it remains difficult to study the functional contribution of a strain in the context of a native-scale community.

In thinking about where to start, two considerations led to the same idea. First, we were concerned about functional redundancy[11,12]. If we drop out a single strain, will we fail to see a phenotype because a strain with a similar function is present in the community? Second, the intestinal ecosystem is organized into physical and metabolic niches, which are thought to serve as functional units within the community[11,12]. A long-standing set of questions concerns how strains function within a niche. What is the mapping of strains to niches? Can changes in one niche propagate to others? And how do these events govern emergent behaviors such as community composition and metabolic output?

Taking these considerations into account, we decided to interrogate a niche rather than an individual strain. Given our interest in the chemistry of the microbiome, we focused on a well-studied microbial pathway—bile acid 7α-dehydroxylation—reasoning that it fits the definition of a metabolic niche since it offers a fitness advantage to a limited set of species that are specialized for bile acid utilization[13,14]. The products of this niche are a highly concentrated pool of metabolites with important biological activities[13–15], but the interactions among its constituent species are poorly understood.

We took advantage of a recently developed model system for the gut microbiome that is composed of >100 of the most common gut bacterial species[16] (Table S1). We find that the niche consists of two species, *Clostridium scindens* (*Cs*) and *Clostridium hylemonae* (*Ch*); when we drop them out of the community together (Δ*Cs*Δ*Ch*), eight strains go up or down sharply in relative abundance. Single-strain dropout communities (Δ*Cs* and Δ*Ch*) reveal that either strain alone can metabolize bile acids exhaustively, and compensation within the niche keeps the relative abundance of its members within a narrow range. They also enable us to test causality in each strain-strain interaction, establishing whether it is specific to *Cs* or *Ch* or a function of both strains. Δ*Cs*- and Δ*Ch*-colonized mice have similar bile acid profiles but a large and unexpected difference in phenylalanine metabolism owing to a *Cs*-specific interaction with *Clostridium sporogenes*, showing that a strain swap within a niche can have a cascading effect that impacts unrelated niches. These data show that a highly controlled experiment can be performed on a complex community to elucidate strain-level causality and mechanism.

Reproducible colonization of a complex gut bacterial community in germ-free mice

The model microbiome we used in this work is based on a recently developed 104-member defined community, hCom1[16]. We included 3 additional strains—*Turicibacter sanguinis* DSM 14220, *Lactobacillus plantarum* WCFS1, and *Clostridium sp.* D5—to improve the community's metabolic potential, resulting a 107-member community (hereafter, hCom1a) (Figure S1).

To test the technical and biological reproducibility of hCom1a colonization in C57BL/6N mice, we used three groups of mice colonized by replicates of hCom1a constructed independently on different days. We gavaged germ-free C57BL/6N mice with thawed aliquots of the frozen community (Figure 1A). After four weeks of colonization, mice were sacrificed and cecal and colonic contents were analyzed by high-resolution metagenomic sequencing (Table S2). Strain abundances in all technical replicates were highly similar in the cecum (pairwise Pearson's R=0.94±0.04). The cecal communities in three groups of biological replicates were very similar in relative abundance profiles (R >0.87 between all pairs, Figure 1B). This high degree of reproducibility supports the use of hCom1a as an experimental model in C57BL/6N mice.

Our analysis of the community composition in all C57BL/6N mice as well as the inoculum yielded four conclusions: 1) We confirmed the presence of almost all strains in the inoculum. Of these, 101 strains were detected with a mean relative abundance >1e-6. Two strains showed a low relative abundance (*Anaerofustis stercorihominis* DSM 17244, *Blautia hydrogenotrophica* DSM 10507) and four others were not detected in all three replicates (*Clostridium methylpentosum* DSM 5476, *Dialister invisus* DSM 15470, *Ethanoligenens harbinense* YUAN-3, *Eubacterium dolichum* DSM 3991) (Figure 1C). 2) Most strains in the inoculum colonized the mouse gut. 96 strains were detected in the mice cecum at least once; of these, 83 strains were detected with a mean relative abundance >1e-6 (Figure 1D). 3) Strain relative abundances were tightly distributed in the inoculum but spanned >6 orders of magnitude in the cecum with a coefficient of variation (CV, standard deviation/mean) <0.4 for nearly all strains (Figure 1C–D). The four strains with variable relative abundances are *Bacteroides sp*. 2-1-22, *Ruminococcus bromii* ATCC 27255, *Slackia heliotrinireducens* DSM 20476, and *Mitsuokella multacida* DSM 20544. 4) All 5 bacterial phyla were observed in the cecum. Bacteroidetes dominated, accounting for 58.2% of total reads, followed by Firmicutes (34.7%), Verrucomicrobia (3.1%), Proteobacteria (0.5%) and Actinobacteria (0.5%) (Figure 1C–D). Taken together, these data show that hCom1a can colonize GF C57BL/6N mice in a highly reproducible manner, facilitating the strain dropout experiments described in this manuscript.

A computational search to identify strains that carry out bile acid 7α-dehydroxylation

Of the strains in hCom1a, only *Clostridium scindens* ATCC 35704 (*Cs*) and *Clostridium hylemonae* DSM 15053 (*Ch*) were known to produce secondary bile acids[14]. Next, we determined whether any additional strains in hCom1a are part of the 7α-dehydroxylation niche. To address this question, we performed a multigeneblast search against a database of genome sequences from hCom1a for the eight-gene *bai* operon (Figure 2A), which encodes a metabolic pathway for the 7α-dehydroxylation of cholic acid (CA) and chenodeoxycholic acid (CDCA) to deoxycholic acid (DCA) and lithocholic acid (LCA), respectively[13] (Figure 2B). Of the 107 strains, only *Cs* and *Ch* harbor the bai operon.

We then sought to test whether any additional strains in the community harbor an alternative (unknown) pathway. We constructed hCom1a and a Δ*Ch*Δ*Cs* dropout community by mixing individually cultured strains, and then we grew these communities in the presence of CA and profiled their culture supernatants by LC-MS. We find that hCom1a converts CA to DCA

whereas Δ*Ch*Δ*Cs* does not (Figure 2C). These data suggest that *Cs* and *Ch* are the only strains in the 7α-dehydroxylation niche, but they do not exclude the possibility that another strain in hCom1a is capable of carrying out this reaction in vivo. By analyzing publicly available human metagenomic data[17], we observe that *Cs* and *Ch* often co-exist in the gut community, indicating that they are not competitively exclusive in the human gut (Figure 2D, Table S1).

Determining the occupancy of the 7α-dehydroxylation niche in vivo

To test whether *Cs* and *Ch* are the only occupants of the 7α-dehydroxylation niche, we colonized germ-free C57BL/6 mice with hCom1a or the two-strain dropout community (Δ*Ch*Δ*Cs*). After three weeks, we sacrificed the mice, harvested intestinal contents, and subjected the samples to targeted metabolomic and high-resolution metagenomic analysis[16] (Figure 3A). By analyzing metagenomic data, we verified the absence of *Cs* and *Ch* in cecal samples from the Δ*Ch*Δ*Cs*-colonized mice (Figure 3B and S2A, Table S3).

The removal of *Ch* and *Cs* has a large impact on the bile acid pool (Figure 3C, Table S4). The products of 7α-dehydroxylation—the secondary bile acids DCA and LCA—are absent in fecal pellets from the Δ*Ch*Δ*Cs* mice, as are prominent derivatives including isoDCA and 3-oxo-DCA. In contrast, Δ*Ch*Δ*Cs* mice have a higher level of the pathway intermediates 7β-CA and 7-oxo-CA and the CDCA epimer ursodeoxycholic acid (UDCA) (Figure 3C). Together, these data suggest *Cs* and *Ch* are the only strains in the 7α-dehydroxylation niche and that dropping them out results in the complete elimination of secondary bile acids. Previous attempts to knock out secondary bile acid production were conducted in the context of simple defined communities[5,6,8,10] or by antibiotic knockdown of resident colonists followed by colonization with an antibiotic-resistant mutant, which depletes a variety of other strains in the community[18]. In contrast, our system is a defined knockout of 7α-dehydroxylation in the setting of a complex community.

Eliminating *Cs* and *Ch* has a large impact on a subset of strains

Next, we sought to assess the ecological impact of *Cs*/*Ch* removal on the rest of the community. Removing a species from a natural ecosystem can have consequences that are difficult to predict[19,20]. In mice, species have been removed from simple defined communities[5,6,10,21] or from undefined communities using antibiotic pretreatment and phage[22], but it remains unclear what effect species removal will have on a complex, unperturbed community in its native setting.

hCom1a and Δ*Ch*Δ*Cs* assume a broadly similar composition in mice (R=0.84) (Figure 3D, Table S3). While 97/107 of the community members have a similar relative abundance, the removal of *Cs* and *Ch* has a striking effect on a subset of eight strains, using a strict threshold of q<0.01 and fold change >100 (Figure 3D–E). *Veillonella sp*. 3-1-44 (*Vs*), *Clostridium sporogenes* (*Cspo*), and *Dorea longicatena* (*Dl*) went up sharply in relative abundance, while *Ruminococcus obeum* (*Ro*), *Ruminococcus bromii* (*Rb*), *Mitsuokella multacida* (*Mm*), *Roseburia intestinalis* (*Ri*), and *Eubacterium ventriosum* (*Ev*) decreased (Figures 3D and S2). Thus, at least in this case, the removal of two strains from a complex

gut community has a large effect on a confined subset of strains that lie outside the 7α-dehydroxylation niche.

Compensation and functional redundancy within the 7α-dehydroxylation niche

To gain more resolution into the interactions within the 7α-dehydroxylation niche, we constructed two new communities—Δ*Ch* and Δ*Cs*—in which the 7α-dehydroxylation niche is occupied by *Cs* or *Ch*, but not both. We colonized germ-free C57BL/6 mice with each of these communities or the parental community (hCom1a) and sampled fecal pellets weekly for three weeks. We then sacrificed the mice, harvested intestinal contents, and subjected all the samples to bile acid profiling and metagenomic sequencing with high-resolution read mapping (Figure 4A).

First, we validated that *Ch* and *Cs* were absent from their respective dropout communities in the cecal samples from week 3 (Figure 4B and S2, Table S3). Next, we analyzed the interactions within the niche by metagenomic sequence analysis. In hCom1a, the relative abundances of *Cs* and *Ch* are ~10^{-3} and ~10^{-4}, respectively. Consistent with the human data (Figure 2D), *Cs* is present at a higher relative abundance than *Ch* when they co-occupy the niche. In the absence of *Cs, Ch* goes up 12-fold in relative abundance; likewise, but to a lesser extent, *Cs* is more abundant in the Δ*Ch* community (Figure 4B). Thus, *Cs* and *Ch* can co-exist, but compensation within the niche keeps the total relative abundance of its residents at a similar level (1.0×10^{-3} in hCom1a, 5.1×10^{-4} in Δ*Cs*, and 1.5×10^{-3} in Δ*Ch*) (Figure S2).

Finally, we quantified the cecal bile acid pool by LC-MS (Figures 4C and S3A, Table S4). The bile acid profiles of Δ*Ch*, Δ*Cs*, and the parental (hCom1a) community are remarkably similar: CA, DCA, and their derivatives (7-oxoCA, 7β-CA, 3-oxoDCA, and isoDCA) are all produced at comparable levels (Figure 4D and S3A). Thus, in the context of a complete community, either strain can carry out the core function of the niche—the conversion of primary to secondary bile acids—on its own.

Single-strain dropouts reveal complex interactions among *Cs*, *Ch*, and interacting strains

Next, we turned to effects outside the 7α-dehydroxylation niche. To test whether the strain-level interactions observed in the Δ*Ch*Δ*Cs* community are caused by *Cs* or *Ch*, we compared metagenomic data from hCom1a-colonized mice with that of Δ*Cs*- and Δ*Ch*-colonized mice to assess the relative abundances of the rest of the strains in the community (Figure 5A, Table S3). The compositions of Δ*Cs* and Δ*Ch* are very similar to that of hCom1a (R=0.86 and 0.88, respectively) (Figure 5B–C). Interestingly, of the eight strains whose relative abundances increased or decreased by >100-fold in the Δ*Ch*Δ*Cs* community, five respond to the absence of *Cs* (*Vs* and *Cspo* ↑; *Ro, Rb*, and *Mm* ↓) and three are impacted by the absence of *Ch* (*Vs* ↑; *Ri* and *Mm* ↓) (Figure 5B–C and S2). These sets overlap partially, suggesting that certain interactions share a common mechanism while others are *Cs*- or *Ch*-specific.

To explore the interaction network around the 7α-dehydroxylation niche in more detail, we combined and clustered the metagenomics data from *Cs, Ch*, and each of the 8 affected strains (Figure 5D). The data are consistent with a model in which strains are linked to the niche in one of three ways: 1) Some strains are specific to *Cs* (*Rb, Ro*, and *Cspo*) or

Ch (*Ri*); these interactions are presumably strain-specific and unrelated to bile acids. 2) *Ev* and *Dl* only respond to the double-strain dropout, indicating a mechanism shared by *Cs* and *Ch*, possibly related to secondary bile acid production. 3) The remaining strains, *Mm* and *Vs*, respond when either or both strains are missing, suggesting a requirement for the simultaneous presence of *Cs* and *Ch* (Figure 5E). We note that we cannot distinguish between direct interactions with *Cs* and/or *Ch* and indirect interactions that involve a third strain. Nevertheless, this analysis demonstrates the power of single-strain dropouts in discovering strain-strain interactions in a complex community.

Dl growth is inhibited by a product of 7α-dehydroxylation

Next, we sought to gain insight into the mechanisms that govern the negative (inhibitory) interactions revealed by this analysis. We focused on *Dorea longicatena* (*Dl*) and *Clostridium sporogenes* (*Cspo*) since *Veillonella sp.* 3-1-44 (*Vs*) did not grow robustly in vitro. *Dl* is only detectable in vivo when *Cs* and *Ch* are both absent, so we reasoned that either *Cs* or *Ch* should be capable of inhibiting its growth. We hypothesized that this growth inhibition is mediated by secondary bile acids, which are produced by both strains. To test this hypothesis, we cultured *Dl* (and, as a control, *Cspo*) in growth medium supplemented with CA and DCA at concentrations ranging from 39 μM-1.25 mM; CDCA and LCA were not considered due to poor solubility at high concentrations. The growth of *Dl* is completely inhibited by DCA at 625 μM, a physiological concentration, while *Cspo* was only partially affected (Figure S4A). In contrast, neither strain was affected by CA at concentrations as high as 1.25 mM (Figure S4B). These results suggest that DCA, which is produced by *Cs* and *Ch*, inhibits colonization by *Dl*.

Investigating the mechanism of the interaction between *Cs* and *Cspo*

We started by testing the hypothesis that a diffusible molecule produced by *Cs* inhibits the growth of *C. sporogenes*. We ruled out the possibility that this molecule is DCA in two ways: we observed that the interaction is specific to *Cs* but not *Ch* (Figure 5), even though both strains produce DCA; and we showed directly that DCA does not inhibit the growth of *C. sporogenes* (Figure S4A). Next, we considered the possibility that the antibacterial metabolite is 1-acetyl-β-carboline (AbC). *C. scindens* has been reported to produce AbC, which inhibits the growth of *C. difficile* and other gut bacterial species in vitro[23]. While DCA has a mild inhibitory effect at high concentrations, AbC has no effect on the growth of *C. sporogenes*, even at concentrations as high as 100–500 μM (higher than reported in the literature) (Figure S4C). Follow-up experiments in which *C. sporogenes* was grown in the presence of spent *Cs* culture medium (Figure 6A) suggest that—at least under the conditions tested here—*Cs* does not produce a diffusible molecule that inhibits the growth of *C. sporogenes*.

We next considered the possibility that the interaction between *C. scindens* and *C. sporogenes* results from competition for a nutrient. *C. sporogenes* specializes in metabolizing amino acids[24,25], so we focused our efforts on amino acid utilization. We started by profiling amino acid levels in the cecum of mice colonized by hCom1a, Δ*Cs*, Δ*Ch*, and Δ*Ch*Δ*Cs*. Though the levels of all amino acids are largely similar among all

groups, arginine, histidine, and tryptophan are at very low levels in the cecum, suggesting their limiting availabilities (Figure 6B).

Since arginine is known to be a particularly important amino acid for *C. sporogenes*[16,26], we considered the possibility that competition for arginine underlies the interaction between *C. scindens* and *C. sporogenes*. To test this hypothesis in an unbiased way, we systematically screened amino acid consumption by every strain in the community (Figure 6C). *C. scindens* did not consume arginine at all, so we considered a second possibility: that the interaction between *C. scindens* and *C. sporogenes* is centered around arginine but is indirect (i.e., involves an intermediary organism).

Among the arginine consumers in our community, *Ruminococcus* caught our attention since all 7 *Ruminococcus* species depleted arginine to some extent (Figure 6C). Notably, *Ruminococcus bromii* (*Rb*) *and Ruminococcus obeum* (*Ro*) respond strongly to *Cs* dropout but in the opposite direction to that of *C. sporogenes*; i.e., like *Cs*, the relative abundance of *Rb* and *Ro* is strongly negatively correlated with that of *C. sporogenes* (Figure S2). While *Ro* depletes about half of the arginine in the medium, *Rb* completely consumes all of the arginine (Figure 6C). These data are consistent with the possibility that *Rb* and *Ro* might compete with *C. sporogenes* for the consumption of arginine *in vivo*.

An unexpected impact of Cs on aromatic amino acid metabolism

The data from Δ*Cs*- and Δ*Ch*-colonized mice suggest that although *Ch* and *Cs* appear functionally redundant within their niche—the two strains are interchangeable in terms of the resulting bile acid profile—they have distinct effects on the rest of the community. However, there are only six strains whose relative abundances are meaningfully different between the Δ*Ch* and Δ*Cs* communities (*Bx, Ri*, *Rb*, *Ro*, *Mm*, and *Cspo*); apart from these, the relative abundances of the rest of the community are nearly superimposable (Figure S5A, Table S3). To determine whether the Δ*Ch* and Δ*Cs* communities are truly indistinguishable, we compared microbiome-derived metabolites in the cecal contents and urine of the Δ*Ch*- and Δ*Cs*-colonized mice, expecting to find concordant profiles in light of the compositional similarities (Figure 7A).

To our surprise, there were striking differences among the profiles (Figure 7B, Table S4). First, three reductive phenylalanine metabolites—phenylpropionic acid, hippuric acid, and cinnamoylglycine—were produced abundantly in Δ*Cs*-colonized mice, but at very low levels in Δ*Ch*- and hCom1a-colonized mice (Figure 7C and S3B–D). Three observations suggest a causal role for *Cspo:* it is the only strain that is essentially undetectable in Δ*Ch*- and hCom1a-colonized mice but up >1000-fold in Δ*Cs*-colonized mice (Figure 5D and 7D), it is the only strain in hCom1a known to produce reductive phenylalanine metabolites in vitro and in vivo[24,27], and its dropout from Δ*Cs*-colonized mice results in a decrease in reductive phenylalanine metabolites (Figure S6).

Second, two oxidative metabolites of phenylalanine—phenylacetic acid and phenylacetylglycine—show the opposite pattern (Figure 7C and S3B–D). Given that reductive and oxidative pathways are competing since they share phenylalanine as a

substrate[24], the decrease in oxidative metabolites likely results from the increase in *C. sporogenes*-mediated reductive metabolism.

These data are consistent with a model in which a strain swap (Δ*Ch vs* Δ*Cs*) initiated a multi-step process that cascaded through the community: *Cs* was replaced with *Ch*, which increased the relative abundance of *Cspo* from nearly undetectable to ~10^{-4}, which increased the level of hippurate (~16 fold) and cinnamoylglycine (~37 fold), which decreased the production of phenylacetate (~2 fold) and phenylacetylglycine (~6 fold) (Figure S5B).

This is especially notable in light of the biological activities of the metabolites involved. Phenylacetylglycine, which plays a causative role in cardiovascular disease[28], is down substantially in Δ*Cs*-colonized mice. It is replaced by hippuric acid and cinnamoylglycine, which are notable for their lack of toxicity[29,30]. Replacing *Cs* with *Ch* results in a 133-fold difference in the ratio of favorable (hippurate and cinnamoylglycine) to unfavorable (phenylacetylglycine) Phe metabolites. Thus, a strain swap in the 7α-dehydroxylation niche is 'silent' in terms of bile acids but yields a large, desirable effect in an unrelated compartment of the community.

DISCUSSION

A long-standing challenge in microbiome research has been to assess the impact of individual strains on community ecology and host physiology. Pioneering efforts have focused on interactions in binary culture[31,32] or in simple communities[33,34], where the rules and selective conditions are likely distinct from those in a complex community[35]. A complex defined community offers a setting in which a 'clean' dropout can be constructed in a physiologically relevant background. This approach, in combination with recent advances in genetic systems for the microbiome[18,25,36], will greatly improve our understanding of strain-strain and strain-host interactions.

Our results emphasize the importance of focusing on a functional unit within the community —here, a metabolic niche—rather than on individual strains. Initially, our main focus was to characterize the effects of secondary bile acids on the host, and our interest in the niche was driven mainly by the concern that the phenotype induced by dropping out a single bile-acid-producing colonist would be masked by another functionally redundant strain. But as we began analyzing metagenomic and metabolomic data from the strain dropout experiments, we came to think that the main story was the connection between ecological interactions and community metabolism.

Using this model, we show that there is functional redundancy within the 7α-dehydroxylation niche. An unknown mechanism—we speculate that it could be the availability of the primary bile acids CA and CDCA—keeps the total relative abundance of strains in the niche within a 3-fold range, regardless of whether the niche is mono- or bi-colonized. *Cs* and *Ch* can co-occupy the niche rather than excluding each other. However, when the niche is mono-colonized, *Cs* and *Ch* are functionally interchangeable; either strain

alone is capable of dehydroxylating the entire pool of primary bile acids, and the resulting bile acid profiles are indistinguishable.

However, changes in the occupancy of the niche lead to unexpected effects elsewhere in the community. Communities in which the niche is mono-colonized with *Cs* (Δ*Ch*) vs. *Ch* (Δ*Cs*) are extremely similar in terms of composition—only six strains differ significantly in relative abundance. But in Δ*Cs*, the unexpected proliferation of *Clostridium sporogenes* —which is below the limit of detection in hCom1a and Δ*Ch*—led to a large increase in reductive phenylalanine metabolites, reshaping the chemical output of a different niche in the community. This finding has two important implications. First, it highlights the functional impact of species- and strain-level variation in the microbiome. Different species that fill the same niche—even those that appear functionally redundant—may yield a large difference outside the niche.

Second, this has important implications for understanding the principles of rational community design. An emerging goal in microbiome research is to design microbial communities that are endowed with an immunologic or metabolic phenotype of interest[37]. If the goal is to make a community that generates hippurate and not phenylacetylglycine, the obvious strategy would be to include strains that produce the former and exclude those that generate the latter. But by dropping out a strain in an unrelated niche, we observed a comparable difference to what we would have expected through rational engineering—and through a simpler maneuver that does not reduce diversity or compromise any other niche. Thus, to alter a phenotype of interest, one needs to consider not just the strains that carry it out but their interaction partners in the community.

LIMITATIONS OF THE STUDY

As a model microbiome, hCom1a has two main limitations in the context of this study. First, it produces a smaller quantity of secondary bile acids than a human fecal community (Figure S7), indicating the possibility of missing strain(s) that could improve bile acid metabolism. hCom2, a derivative of hCom1, is more comparable to a human fecal community[16] and could be used for subsequent strain dropout studies. Second, hCom1a is only one community; there is substantial strain- and species-level variation among human microbiomes, so the interactions discovered here may not exist in other communities.

Our experimental findings have two additional limitations. Although we explored the interaction between *Cs* and *C. sporogenes* in detail and present evidence consistent with an indirect competition for arginine (Figures 6 and S4), our data are not sufficient to establish the mechanism; further studies in which *Ro* and/or *Rb* are dropped out, alone and in combination with *C. sporogenes*, would be required, as would experiments in which arginine levels are modulated.

Our experimental setup and data interpretation may imply an overly simplistic view in which bacterial species belong to an individual niche. In reality, strains occupy multiple niches simultaneously. We hope that an approach similar to the one employed here can be used to

explore the way in which strains map to niches, and strain-strain interactions yield effects across multiple niches.

STAR★METHODS

RESOURCE AVAILABILITY

Lead contact—Further information and requests for resources and reagents should be directed to and will be fulfilled by the lead contact, Michael Fischbach (fischbach@fischbachgroup.org).

Materials availability—The bacterial strains used in this study are available from the sources listed in the Key Resources Table.

Data and code availability

- Metagenomic sequencing datasets generated for this study have been deposited at the NCBI Sequence Read Archive and are publicly available as of the date of publication. Accession numbers are listed in the Key Resources Table. Metabolomics data have been deposited on the ProteomeXchange Consortium via the MassIVE database and are publicly available as of the date of publication. Accession numbers are also listed in the Key Resources Table. All data reported in this paper will be shared by the lead contact upon request.
- This paper does not report any original code. All computational approaches and software used are described in the STAR Methods and listed Key Resources Table.
- Any additional information required to reanalyze the data reported in this paper is available from the lead contact upon request.

EXPERIMENTAL MODEL AND SUBJECT DETAILS

Bacterial strains and culture conditions—All strains used in the synthetic community were obtained from American Type Culture Collection (ATCC), Leibniz Institute DSMZ-German Collection of Microorganisms and Cell Cultures GmbH (DSMZ), BEI resources (BEI), and other sources as indicated in Table S1. All strains were cultured in one of two growth media: mega medium (MM) and chopped meat medium w/ rumen fluid and carbohydrates (CMM) (Table S1). Cultures were incubated at 37 °C in an anaerobic chamber (Coy Laboratories) in an atmosphere of 5% hydrogen, 10% CO_2 and 85% N_2. Cultures were stored in anaerobically prepared 25% glycerol/water (v/v) in 12.7 × 49 mm cryogenic vials with closures (Corning 430659) or 1.2 ml V-bottom 96-well plates (Thomas Scientific, OX1263-S) capped with a plate seal (Thomas Scientific, EK-2066) and sealed with oxygen-impervious yellow vinyl tape (Coy Laboratories, 1600330w) to ensure anoxic conditions during long-term storage. All medium and reagents used in the anaerobic chamber were pre-reduced for at least 48 h.

Synthetic community construction—Frozen stocks in a 96-well plate were thawed, and 100 μl of each thawed culture was used to inoculate 1 ml of growth medium (Table S1)

in a sterile 2.2 ml 96-well plate (Thomas Scientific, OX1265-S). Strains were sub-cultured by 1:10 dilution into fresh medium daily for 2–3 days; growth was monitored by optical density at 600 nm (OD_{600}) using a microplate spectrophotometer (BioTeK, Epoch2). For each batch of inoculum, a few strains (typically <10) had a low OD (<0.1). For these strains, additional cells were harvested and added from a 10 ml liquid culture prepared from a glycerol stock, or from single colonies scraped from solid growth medium. Finally, non-normalized cultures of all strains were pooled into a mixture. A 1 ml aliquot of the resulting mixed culture was stored at −80 °C for metagenomic sequencing. The remainder of the mixed culture was subjected to centrifugation (5000 × *g*, 15 min); the cell pellet was washed with an equal volume of pre-reduced sterile phosphate-buffered saline (PBS), and then resuspended in 1/10 of the initial volume of a 25% glycerol/water (v/v) solution. 1.2 ml aliquots of the resulting synthetic community were stored in 2 ml cryovials (Corning, 430659) at −80 °C until use.

Gnotobiotic mouse experiments—Germ free Swiss-Webster or C57BL/6N mice (male, 6–8 weeks of age) were originally obtained from Taconic Biosciences (Hudson, NY) and colonies were maintained in gnotobiotic isolators and fed ad libitum. The Institutional Animal Care and Use Committee (IACUC) at Stanford University approved all procedures involving animals.

Glycerol stocks of synthetic communities (~1.2 ml) were thawed and shaken well at room temperature, and mice were orally gavaged with ~200 μl of the mixed culture. To ensure efficient colonization by all strains in the community, mice were gavaged using the same procedure on three successive days for all experiments. Human stool homogenates were prepared in PBS and administered by gavage to germ-free mice using the same protocol as the synthetic community.

For experiments in which Swiss-Webster or C57BL/6N mice were fed standard chow (LabDiet 5k67), fresh fecal pellets were collected weekly at the same time of day and stored at −80 °C prior to analysis. The mice were maintained on a standard diet (LabDiet 5k67; 0.2% Trp) for 4 weeks (unless otherwise stated) before sacrifice (fed ad libitum). Mice were euthanized humanely by CO_2 asphyxiation and the luminal contents of the small intestine, cecum, and colon were collected at the same time of day and stored at −80 °C until use.

METHOD DETAILS

Metagenomic sequencing—The same experimental pipeline was used for sequencing bacterial isolates and microbial communities. Bacterial cells were pelleted by centrifugation in an anaerobic environment. To estimate the absolute abundance of all strains in the communities, 100 μl of bacterial suspension containing 10^5 cells of *Paenibacillus barengoltzii* CC33–002B was added to each sample prior DNA extraction. Genomic DNA was extracted using the DNeasy PowerSoil HTP kit (Qiagen) and the quantity of extracted genomic DNA was measured in a 384-well format using the Quant-iT PicoGreen dsDNA Assay Kit (Thermo Fisher). Sequencing libraries were generated in a 384-well format using a custom, low-volume protocol based on the Nextera XT process (Illumina). Briefly, the DNA concentration from each sample was normalized to 0.18 ng/μl using a Mantis liquid

handler (Formulatrix). In cases where the concentration was below 0.18 ng/μl, the sample was not diluted further. Tagmentation, neutralization, and PCR steps of the Nextera XT process were performed on the Mosquito HTS liquid handler (TTP Labtech), creating a final volume of 4 μl per library. During the PCR amplification step, custom 12-bp dual unique indices were introduced to eliminate barcode switching, a phenomenon that occurs on Illumina sequencing platforms with patterned flow cells[38]. Libraries were pooled at the desired relative molar ratios and cleaned up using Ampure XP beads (Beckman) to effect buffer removal and library size selection. The cleanup process was used to remove fragments shorter than 300 bp and longer than 1.5 kb. Final library pools were quality checked for size distribution and concentration using the Fragment Analyzer (Agilent) and qPCR (BioRad). Sequencing reads were generated using the NovaSeq S4 flow cell or the NextSeq High Output kit, both in 2×150 bp configuration. 5–10 million paired-end reads were targeted for bacterial isolates and 20–30 million paired end reads for bacterial communities.

Metagenomic read mapping—Paired-end reads from each sample were aligned to the hCom1a database using Bowtie2[39] with maximum insert length (-maxins) set to 3000, maximum alignments (-k) set to 300, suppressed unpaired alignments (--no-mixed), suppressed discordant alignments (--no-discordant), suppressed output for unaligned reads (--no-unal), required global alignment (--end-to-end), and using the "--very-sensitive" alignment preset (command: --very-sensitive -maxinsX 3000 -k 300 --no-mixed --no-discordant --end-to-end --no-unal). The output was piped into Samtools v. 1.9[40], which was used to convert the alignment output from SAM output stream to BAM format and then sort and index the BAM file by coordinates. Alignments were filtered to only keep those with >99% identity for the entire length of the read.

The median percentage of unaligned reads was 4.95% (range 4.10% – 8.35%). To assess the origin of these reads, we performed a BLAST v2.11.0+ search through the ncbi/blast:latest docker image with parameters "-outfmt '6 std qlen slen qcovs sscinames staxids' -dbsize 1000000, -num_alignments 100" from a representative sample against the 'NCBI - nt' database as on 2021-02-16. We then filtered the BLAST results to obtain the top hits for a given query. Briefly, the script defined top hits as ones that had an e-value <= 1e-30, percent identity >= 99% and were within 10 percent of the best bit score for that query. To visualize and summarize the output, we used the ktImportTaxonomy script from the Krona package with default parameters. Reads were aggregated by NCBI taxon id and separately by genus. We found that most of the hits are from taxa that are closely related to the organisms in our community, while others are from the mouse genome. We conclude that our experiments did not suffer from any appreciable level of contamination.

Sample preparation for LC/MS—For mouse fecal samples (~40 mg) or cecal contents and liver (~80 mg), wet tissues were pre-weighed into a 2 ml screw top tube containing six 6 mm ceramic beads (Precellys® CK28 Lysing Kit). 600 μL (for fecal samples) or 1 ml (for cecal contents and liver) of a mixture of ice-cold acetonitrile, methanol, and water (4/4/2, v/v/v) was then added to each tube and samples were homogenized by vigorous shaking using a QIAGEN Tissue Lyser II at 25/s for 10 min. The resulting homogenates were subjected to centrifugation for 15 min at 4 °C at 18,000 × *g*. 100 μl of the supernatant

was then combined with 100 μl of aqueous solution of internal standards (2 μM d^4-cholic acid and 20 μM 4-chloro-L-phenylalanine). The resulting mixtures were then filtered through a Durapore PVDF 0.22-μm membrane using Ultrafree centrifugal filters (Millipore, UFC30GV00), or MultiScreen Solvinert 96 Well Filter Plate (Millipore, MSRLN0410), and 5 μl was injected into the LC/MS.

For mouse urine samples, 5 μl of a urine sample was diluted 10-fold with ddH_2O and then mixed with 50 μl of an aqueous internal standard solution (20 μM 4-chloro-L-phenylalanine). After centrifugation for 15 min at 4 °C at 18,000 × *g*, 50 μl of the resulting mixture was used for quantification of creatinine using a Creatinine Assay Kit (ab204537) as described in the manufacturer's protocol. The remaining 50 μl of each sample was filtered through a Durapore PVDF 0.22-μm membrane using Ultrafree centrifugal filters (Millipore, UFC30GV00), and 5 μl was injected into the LC/MS.

For mouse serum or plasma samples, protein was precipitated by mixing blood samples (50 μl) with an equal volume of 6% aqueous sulfosalicylic acid, followed by incubation at room temperature for 5 min and clarification by centrifugation (18,000 × g, 10 min, room temperature). Subsequently, 50 μl of the supernatant was combined with 50 μl of aqueous solution of internal standards (2 μM d^4-cholic acid and 20 μM 4-chloro-L-phenylalanine). The resulting mixtures were then filtered through a Durapore PVDF 0.22-μm membrane using Ultrafree centrifugal filters (Millipore, UFC30GV00), and 5 μl was injected into the LC/MS.

For bacterial (community) cultures, 200 μl of each sample was transferred into individual 1.5 ml microtubes or 1.2 ml 96 well plates and then centrifuged for 15 min at 4 °C at 18,000 × g or 3,700 × g. Subsequently, 100 μl of the supernatant was combined with 100 μL of an aqueous solution of the internal standard (20 μM 4-chloro-L-phenylalanine). The resulting mixtures were filtered through a Durapore PVDF 0.22-μm membrane using Ultrafree centrifugal filters (Millipore, UFC30GV00), or a MultiScreen Solvinert 96 Well Filter Plate (Millipore, MSRLN0410), and 5 μl was injected into the LC/MS.

Liquid chromatography/mass spectrometry (LC/MS)—*Bile acids*: compounds were separated using an Agilent 1290 Infinity II UPLC equipped with a Kinetex C18 column (1.7 μm, 2.1 × 100 mm, Phenomenex) and detected using an Agilent 6530 Q-TOF equipped with a dual Agilent jet stream electrospray ionization (AJS-ESI) source operating under extended dynamic range (EDR 1700 m/z) in negative ionization mode. The parameters of the AJS-ESI source were as follows: gas temp: 300 °C; drying gas: 7.0 l/min; nebulizer: 40 psig; sheath gas temp: 350 °C; sheath gas flow: 10.0 l/min; VCap: 3500 V; nozzle voltage: 1400V; and fragmenter: 200 V. Mobile phase A was 0.05% formic acid in H_2O, and mobile phase B was 0.05% formic acid in acetone. 5 μl of each sample was injected via autosampler into mobile phase and chromatographic separation was carried out at a flow rate of 0.35 ml/min with a 32-min gradient condition (t = 0 min, 25% B; t = 1 min, 25% B; t = 25 min, 75% B, t = 26 min, 100% B, t = 30 min, 100% B, t = 32 min, 25% B).

(Aromatic) amino acid metabolites: compounds were separated using an Agilent 1290 Infinity II UPLC equipped with an ACQUITY UPLC BEH C18 column (1.7 μm, 2.1

mm × 150 mm, Waters) and detected using an Agilent 6530 Q-TOF equipped with a standard atmospheric-pressure chemical ionization (APCI) source or dual Agilent jet stream electrospray ionization (AJS-ESI) source operating under extended dynamic range (EDR 1700 m/z) in negative ionization mode. For the APCI source the parameters were as follows: gas temp: 350 °C; vaporizer: 350 °C; drying gas: 6.0 l/min; nebulizer: 60 psig; VCap: 3500 V; corona: 20 μA; and fragmenter: 135 V. For the AJS-ESI source the parameters were as follows: gas temp: 350 °C; drying gas: 10.0 l/min; nebulizer: 40 psig; sheath gas temp: 300 °C; sheath gas flow: 11.0 l/min; VCap: 3500 V; nozzle voltage: 1400V; and fragmenter: 130 V. Mobile phase A was 6.5 mM ammonium bicarbonate in H_2O, and B was 6.5 mM ammonium bicarbonate in 95 % MeOH/H_2O. 5 μl of each sample was injected via autosampler into mobile phase and chromatographic separation was carried out at a flow rate of 0.35 mL/min with a 10-min gradient condition (t = 0 min, 0.5% B; t = 4 min, 70% B; t = 4.5 min, 98% B; t = 5.4 min, 98% B; t = 5.6 min, 0.5% B).

Online mass calibration was performed using a second ionization source and a constant flow (5 μl/min) of reference solution (119.0363 and 966.0007 m/z). The MassHunter Quantitative Analysis Software (Agilent, version B.09.00) was used for peak integration based on retention time (tolerance of 0.2 min) and accurate m/z (tolerance of 30 ppm) of chemical standards. Quantification was based on a 2-fold dilution series of chemical standards spanning 0.098 to 200 μM (for AAA metabolites) or 0.001 to 200 μM (for bile acids) and measured amounts were normalized by weights of extracted tissue samples (pmol/mg wet tissue) or creatinine level in the urine sample (μM/mM creatinine). The linear quantification range and lower limit of detection for all metabolites are listed in Table S1. The MassHunter Qualitative Analysis Software (Agilent, version 7.0) was used for targeted feature extraction, allowing mass tolerances of 30 ppm.

Bile acids inhibition assay—*D. longicatena* and *C. sporogenes* were streaked from a glycerol stock onto Columbia Agar with 5 % Sheep Blood (BD 221165) and incubated for ~ 24 h at 37 °C. Individual colonies were picked and used to inoculate 3 ml of Mega medium and cultured for 24 h at 37 °C. Cells were diluted 100-fold into fresh Mega medium supplemented with various concentration of CA or DCA (final concentration raging from 1.25 mM, 625 μM, 312 μM, 156 μM, 78 μM, to 39 μM) or DMSO blank control. The starting OD_{600} for each culture was 0.1. 200 μl aliquots of each culture were taken and monitored for growth using an Epoch 2 microplate reader (Biotek) in an anaerobic chamber every 15 min until stationary phase was reached. Bacterial growth curves were performed in triplicate with each biological replicate derived from a single isolated colony. Growth curves were plotted using GraphPad.

1-Acetyl-β-carboline inhibition assay—*C. sporogenes* was streaked from a glycerol stock onto Columbia Agar with 5% Sheep Blood (BD 221165) and incubated for ~24 h at 37 °C. Individual colonies were picked and used to inoculate 3 ml of Mega medium and cultured for 24 h at 37 °C. Cells were diluted 100-fold into fresh Mega medium supplemented with various concentration of AbC or DCA (final concentration raging from 500 μM, 100 μM, 50 μM, 25 μM, to 5 μM) or DMSO blank control. The starting OD_{600} for each culture was ~0.01 after background subtraction. 200 μl aliquots of each culture were

sampled to monitor growth using an Epoch 2 microplate reader (Biotek) in an anaerobic chamber every 30 min until stationary phase was reached. Bacterial growth curves were performed in one biological replicate. Growth curves were plotted using GraphPad.

***C. scindens* and *C. hylemonae* spent medium assay—**Glycerol stocks of *C. scindens* and *C. hylemonae* were used to inoculate 3 ml of Mega medium and cultured for ~24 h at 37 °C. Cells were diluted 100-fold into 7 ml of Peptone Yeast Extract Broth with Fructose (PYF medium, Anaerobe system) and incubated for 24 h at 37 °C. After centrifugation (5000 rpm, 10 min), bacterial supernatants were filtered through a 0.22 μm nylon membrane to remove cell material. The resulting spent medium was extracted 2x with ethyl acetate (EA); the ethyl acetate layer was evaporated to yield the extract, while the aqueous layer was lyophilized to generate the lyophilizate. Finally, we inoculated an overnight culture of *C. sporogenes* into fresh PYF medium or fresh PYF medium supplemented with either the extract or lyophilizate of *C. scindens* or *C. hylemonae*. The growth of *C. sporogenes* was monitored using an Epoch 2 microplate reader (Biotek) in an anaerobic chamber every 30 min until stationary phase was reached. Bacterial growth curves were performed in three biological replicates. Growth curves were plotted using GraphPad.

***In vitro* profiling of amino acids depletion by hCom1a strains—**Glycerol stocks of each strain in hCom1a were used to inoculate 3 ml of rich medium (Mega medium or modified Chopped meat medium); these cultures were incubated 1–4 days at 37 °C. After reaching stationary phase, bacterial cells were harvested by centrifugation (5,000 × g, 10 min), washed twice with an equal volume of pre-reduced sterile phosphate-buffered saline (PBS), and resuspended in 0.75 ml minimal medium with 20 amino acids (modified SAAC medium, see Table S1). The resulting cell suspensions were incubated at 37 °C for another 4 d. All bacterial cultures were stored at −80 °C prior to LC-MS analysis. These samples were used to profile amino acids, 3-phenylpropionic acid, 3-(4-hydrophenyl) propionic acid, and 3-indolepropionic acid.

QUANTIFICATION AND STATISTICAL ANALYSIS

Relative abundances were calculated from the raw output of NinjaMap-processed metagenomic data without rarefying the total number of reads across samples. After setting undetected bins to a minimum value of 10^{-8}, all relative abundances were further transformed by log10. To evaluate the reproducibility of *in vivo* colonization, Pearson's correlation coefficients (R) were calculated for the community structure between each two experiments after averaging the relative abundance of each strain across the 3–5 mice that were co-housed in the same cage/experiment. To find the potential strains significantly impacted by strain(s) dropout, multiple unpaired t test with FDR correction was performed for each strain in all mice between two groups. The statistical parameters were set as default with individual variance computed for each comparison followed by multiple comparison of false discovery rate (FDR) with two-stage step-up (Benjamini, K Krieger, and Yekutieli) and Q=0.1%. Dot plots showing relative abundance data were plotted with a conservative lower threshold of 1×10^{-6}. Further details of statistical analyses can be found in the corresponding figure legends. All statistical analysis and plotting were performed in MATLAB or Prism.

For metabolomic data, metabolite concentration differences between experimental groups or conditions were evaluated using unpaired two-tailed Students' t test for pairwise comparison, one-way ANOVA for multiple comparisons. All statistical analysis and plotting were performed in Prism.

Supplementary Material

Refer to Web version on PubMed Central for supplementary material.

ACKNOWLEDGMENTS

We are deeply indebted to members of the Fischbach, Brown, and Hazen labs for helpful discussions. We are grateful to Mohamed Donia (Princeton) for helpful discussions regarding data analysis, and to Brian Yu (Chan Zuckerberg Biohub) for help with figure preparation. This work was supported by the Human Frontier Science Program LT000493/2018-L (K.N.), a Fellowship from the Astellas Foundation for Research on Metabolic Disorders (K.N.), a research grant from Kanae Fundation for the Promotion of Medical Science (K.N.), the Stanford Microbiome Therapies Initiative (M.A.F.), NIH grants DP1 DK113598 (to M.A.F.), P01 HL147823 (to M.A.F. and J.M.B.), R01 DK101674 (to M.A.F.), P50 AA024333 (J.M.B.), R01 DK130227 (J.M.B.), NSF grant EF-2125383 (M.A.F.) the Bill and Melinda Gates Foundation (to M.A.F.), an HHMI-Simons Faculty Scholars Award (M.A.F.), the Leducq Foundation (M.A.F.), the Leona M. and Harry B. Helmsley Charitable Trust (M.A.F.); and MAC3 Impact Philanthropies (M.A.F.). M.A.F. is a Chan Zuckerberg Biohub Investigator.

INCLUSION AND DIVERSITY

We support inclusive, diverse, and equitable conduct of research.

REFERENCES

1. Samuel BS, and Gordon JI (2006). A humanized gnotobiotic mouse model of host-archaeal-bacterial mutualism. Proc. Natl. Acad. Sci 103, 10011–10016. 10.1073/pnas.0602187103. [PubMed: 16782812]
2. Mahowald MA, Rey FE, Seedorf H, Turnbaugh PJ, Fulton RS, Wollam A, Shah N, Wang C, Magrini V, Wilson RK, et al. (2009). Characterizing a model human gut microbiota composed of members of its two dominant bacterial phyla. Proc. Natl. Acad. Sci 106, 5859–5864. 10.1073/pnas.0901529106. [PubMed: 19321416]
3. Rey FE, Faith JJ, Bain J, Muehlbauer MJ, Stevens RD, Newgard CB, and Gordon JI (2010). Dissecting the in Vivo Metabolic Potential of Two Human Gut Acetogens. J. Biol. Chem 285, 22082–22090. 10.1074/jbc.M110.117713. [PubMed: 20444704]
4. Buffie CG, Bucci V, Stein RR, McKenney PT, Ling L, Gobourne A, No D, Liu H, Kinnebrew M, Viale A, et al. (2014). Precision microbiome reconstitution restores bile acid mediated resistance to Clostridium difficile. Nature 517, 205–208. 10.1038/nature13828. [PubMed: 25337874]
5. Studer N, Desharnais L, Beutler M, Brugiroux S, Terrazos MA, Menin L, Schürch CM, McCoy KD, Kuehne SA, Minton NP, et al. (2016). Functional Intestinal Bile Acid 7α-Dehydroxylation by Clostridium scindens Associated with Protection from Clostridium difficile Infection in a Gnotobiotic Mouse Model. Front. Cell. Infect. Microbiol 6, 1–15. 10.3389/fcimb.2016.00191. [PubMed: 26870699]
6. Marion S, Studer N, Desharnais L, Menin L, Escrig S, Meibom A, Hapfelmeier S, and Bernier-Latmani R (2019). In vitro and in vivo characterization of Clostridium scindens bile acid transformations. Gut Microbes 10, 481–503. 10.1080/19490976.2018.1549420. [PubMed: 30589376]
7. Patnode ML, Beller ZW, Han ND, Cheng J, Peters SL, Terrapon N, Henrissat B, Le Gall S, Saulnier L, Hayashi DK, et al. (2019). Interspecies Competition Impacts Targeted Manipulation of Human Gut Bacteria by Fiber-Derived Glycans. Cell 179, 59–73.e13. 10.1016/j.cell.2019.08.011. [PubMed: 31539500]

8. Marion S, Desharnais L, Studer N, Dong Y, Notter MD, Poudel S, Menin L, Janowczyk A, Hettich RL, Hapfelmeier S, et al. (2020). Biogeography of microbial bile acid transformations along the murine gut. J. Lipid Res 61, 1450–1463. 10.1194/jlr.RA120001021. [PubMed: 32661017]

9. Ridlon JM, Devendran S, Alves JM, Doden H, Wolf PG, Pereira GV, Ly L, Volland A, Takei H, Nittono H, et al. (2020). The 'in vivo lifestyle' of bile acid 7α-dehydroxylating bacteria: comparative genomics, metatranscriptomic, and bile acid metabolomics analysis of a defined microbial community in gnotobiotic mice. Gut Microbes 11, 381–404. 10.1080/19490976.2019.1618173. [PubMed: 31177942]

10. Streidl T, Karkossa I, Segura Muñoz RR, Eberl C, Zaufel A, Plagge J, Schmaltz R, Schubert K, Basic M, Schneider KM, et al. (2021). The gut bacterium Extibacter muris produces secondary bile acids and influences liver physiology in gnotobiotic mice. Gut Microbes 13, 1–21. 10.1080/19490976.2020.1854008.

11. Louca S, Polz MF, Mazel F, Albright MBN, Huber JA, O'Connor MI, Ackermann M, Hahn AS, Srivastava DS, Crowe SA, et al. (2018). Function and functional redundancy in microbial systems. Nat. Ecol. Evol 2, 936–943. 10.1038/s41559-018-0519-1. [PubMed: 29662222]

12. Tian L, Wang X-W, Wu A-K, Fan Y, Friedman J, Dahlin A, Waldor MK, Weinstock GM, Weiss ST, and Liu Y-Y (2020). Deciphering functional redundancy in the human microbiome. Nat. Commun 11, 6217. 10.1038/s41467-020-19940-1. [PubMed: 33277504]

13. Funabashi M, Grove TL, Wang M, Varma Y, McFadden ME, Brown LC, Guo C, Higginbottom S, Almo SC, and Fischbach MA (2020). A metabolic pathway for bile acid dehydroxylation by the gut microbiome. Nature 582, 566–570. 10.1038/s41586-020-2396-4. [PubMed: 32555455]

14. Ridlon JM, Harris SC, Bhowmik S, Kang D-J, and Hylemon PB (2016). Consequences of bile salt biotransformations by intestinal bacteria. Gut Microbes 7, 22–39. 10.1080/19490976.2015.1127483. [PubMed: 26939849]

15. Ridlon JM, Kang D-J, and Hylemon PB (2006). Bile salt biotransformations by human intestinal bacteria. J. Lipid Res 47, 241–259. 10.1194/jlr.R500013-JLR200. [PubMed: 16299351]

16. Cheng AG, Ho P, Aranda-Díaz A, Jain S, Yu FB, Meng X, Wang M, Iakiviak M, Nagashima K, Zhao A, et al. (2022). Design, construction, and in vivo augmentation of a complex gut microbiome. Cell 185, 3617–3636.e19. 10.1016/j.cell.2022.08.003. [PubMed: 36070752]

17. Kraal L, Abubucker S, Kota K, Fischbach MA, and Mitreva M (2014). The Prevalence of Species and Strains in the Human Microbiome: A Resource for Experimental Efforts. PLoS One 9, e97279. 10.1371/journal.pone.0097279. [PubMed: 24827833]

18. Jin W-B, Li T-T, Huo D, Qu S, Li XV, Arifuzzaman M, Lima SF, Shi H-Q, Wang A, Putzel GG, et al. (2022). Genetic manipulation of gut microbes enables single-gene interrogation in a complex microbiome. Cell 185, 547–562.e22. 10.1016/j.cell.2021.12.035. [PubMed: 35051369]

19. Wootton JT (2010). Experimental species removal alters ecological dynamics in a natural ecosystem. Ecology 91, 42–48. 10.1890/08-1868.1. [PubMed: 20380194]

20. Díaz S, Symstad AJ, Stuart Chapin F, Wardle DA, and Huenneke LF (2003). Functional diversity revealed by removal experiments. Trends Ecol. Evol 18, 140–146. 10.1016/S0169-5347(03)00007-7.

21. Marion S, Desharnais L, Studer N, Dong Y, Notter MD, Poudel S, Menin L, Janowczyk A, Hettich RL, Hapfelmeier S, et al. (2020). Biogeography of microbial bile acid transformations along the murine gut. J. Lipid Res 61, 1450–1463. 10.1194/jlr.RA120001021. [PubMed: 32661017]

22. Lam KN, Spanogiannopoulos P, Soto-Perez P, Alexander M, Nalley MJ, Bisanz JE, Nayak RR, Weakley AM, Yu FB, and Turnbaugh PJ (2021). Phage-delivered CRISPR-Cas9 for strain-specific depletion and genomic deletions in the gut microbiome. Cell Rep. 37, 109930. 10.1016/j.celrep.2021.109930. [PubMed: 34731631]

23. Kang JD, Myers CJ, Harris SC, Kakiyama G, Lee I-K, Yun B-S, Matsuzaki K, Furukawa M, Min H-K, Bajaj JS, et al. (2019). Bile Acid 7α-Dehydroxylating Gut Bacteria Secrete Antibiotics that Inhibit Clostridium difficile: Role of Secondary Bile Acids. Cell Chem. Biol 26, 27–34.e4. 10.1016/j.chembiol.2018.10.003. [PubMed: 30482679]

24. Dodd D, Spitzer MH, Van Treuren W, Merrill BD, Hryckowian AJ, Higginbottom SK, Le A, Cowan TM, Nolan GP, Fischbach MA, et al. (2017). A gut bacterial pathway metabolizes aromatic

amino acids into nine circulating metabolites. Nature 551, 648–652. 10.1038/nature24661. [PubMed: 29168502]

25. Guo C, Allen BM, Hiam KJ, Dodd D, Van Treuren W, Higginbottom S, Nagashima K, Fischer CR, Sonnenburg JL, Spitzer MH, et al. (2019). Depletion of microbiome-derived molecules in the host using Clostridium genetics. Science. 366, eaav1282. 10.1126/science.aav1282.
26. Liu Y, Chen H, Van Treuren W, Hou B, Higginbottom SK, and Dodd D (2022). Clostridium sporogenes uses reductive Stickland metabolism in the gut to generate ATP and produce circulating metabolites. Nat. Microbiol 7, 695–706. 10.1038/s41564-022-01109-9. [PubMed: 35505245]
27. Han S, Van Treuren W, Fischer CR, Merrill BD, DeFelice BC, Sanchez JM, Higginbottom SK, Guthrie L, Fall LA, Dodd D, et al. (2021). A metabolomics pipeline for the mechanistic interrogation of the gut microbiome. Nature 595, 415–420. 10.1038/s41586-021-03707-9. [PubMed: 34262212]
28. Nemet I, Saha PP, Gupta N, Zhu W, Romano KA, Skye SM, Cajka T, Mohan ML, Li L, Wu Y, et al. (2020). A Cardiovascular Disease-Linked Gut Microbial Metabolite Acts via Adrenergic Receptors. Cell 180, 862–877.e22. 10.1016/j.cell.2020.02.016. [PubMed: 32142679]
29. Hoskins JA, Holliday SB, and Greenway AM (1984). The metabolism of cinnamic acid by healthy and phenylketonuric adults: A kinetic study. Biol. Mass Spectrom 11, 296–300. 10.1002/bms.1200110609.
30. Lees HJ, Swann JR, Wilson ID, Nicholson JK, and Holmes E (2013). Hippurate: The natural history of a mammalian-microbial cometabolite. J. Proteome Res 12, 1527–1546. 10.1021/pr300900b. [PubMed: 23342949]
31. Medlock GL, Carey MA, McDuffie DG, Mundy MB, Giallourou N, Swann JR, Kolling GL, and Papin JA (2018). Inferring Metabolic Mechanisms of Interaction within a Defined Gut Microbiota. Cell Syst. 7, 245–257.e7. 10.1016/j.cels.2018.08.003. [PubMed: 30195437]
32. Venturelli OS, Carr AV, Fisher G, Hsu RH, Lau R, Bowen BP, Hromada S, Northen T, and Arkin AP (2018). Deciphering microbial interactions in synthetic human gut microbiome communities. Mol. Syst. Biol 14, 1–19. 10.15252/msb.20178157.
33. Sanchez-Gorostiaga A, Bajić D, Osborne ML, Poyatos JF, and Sanchez A (2019). High-order interactions distort the functional landscape of microbial consortia. PLOS Biol. 17, e3000550. 10.1371/journal.pbio.3000550. [PubMed: 31830028]
34. Gutiérrez N, and Garrido D (2019). Species Deletions from Microbiome Consortia Reveal Key Metabolic Interactions between Gut Microbes. mSystems 4, 1–16. 10.1128/mSystems.00185-19.
35. Bairey E, Kelsic ED, and Kishony R (2016). High-order species interactions shape ecosystem diversity. Nat. Commun 7, 12285. 10.1038/ncomms12285. [PubMed: 27481625]
36. García-Bayona L, and Comstock LE (2019). Streamlined Genetic Manipulation of Diverse Bacteroides and Parabacteroides Isolates from the Human Gut Microbiota. MBio 10. 10.1128/mBio.01762-19.
37. Fischbach MA (2018). Microbiome: Focus on Causation and Mechanism. Cell 174, 785–790. 10.1016/j.cell.2018.07.038. [PubMed: 30096310]
38. Sinha R, Stanley G, Gulati GS, Ezran C, Travaglini KJ, Wei E, Chan CKF, Nabhan AN, Su T, Morganti RM, et al. (2017). Index Switching Causes “Spreading-Of-Signal” Among Multiplexed Samples In Illumina HiSeq 4000 DNA Sequencing. bioRxiv, 125724. 10.1101/125724.
39. Langmead B, and Salzberg SL (2012). Fast gapped-read alignment with Bowtie 2. Nat. Methods 9, 357–359. 10.1038/nmeth.1923. [PubMed: 22388286]
40. Li H, Handsaker B, Wysoker A, Fennell T, Ruan J, Homer N, Marth G, Abecasis G, Durbin R, and Subgroup, 1000 Genome Project Data Processing (2009). The Sequence Alignment/Map format and SAMtools. Bioinformatics 25, 2078–2079. 10.1093/bioinformatics/btp352. [PubMed: 19505943]

HIGHLIGHTS

- Construction of variants of a complex community missing two strains in a metabolic niche
- In the Δ*Cs*Δ*Ch* community, eight strains change in relative abundance by >100-fold
- *Clostridium sporogenes* increases >1000-fold in the Δ*Cs* but not Δ*Ch* dropout
- A strain swap can ripple through the community in an unpredictable manner

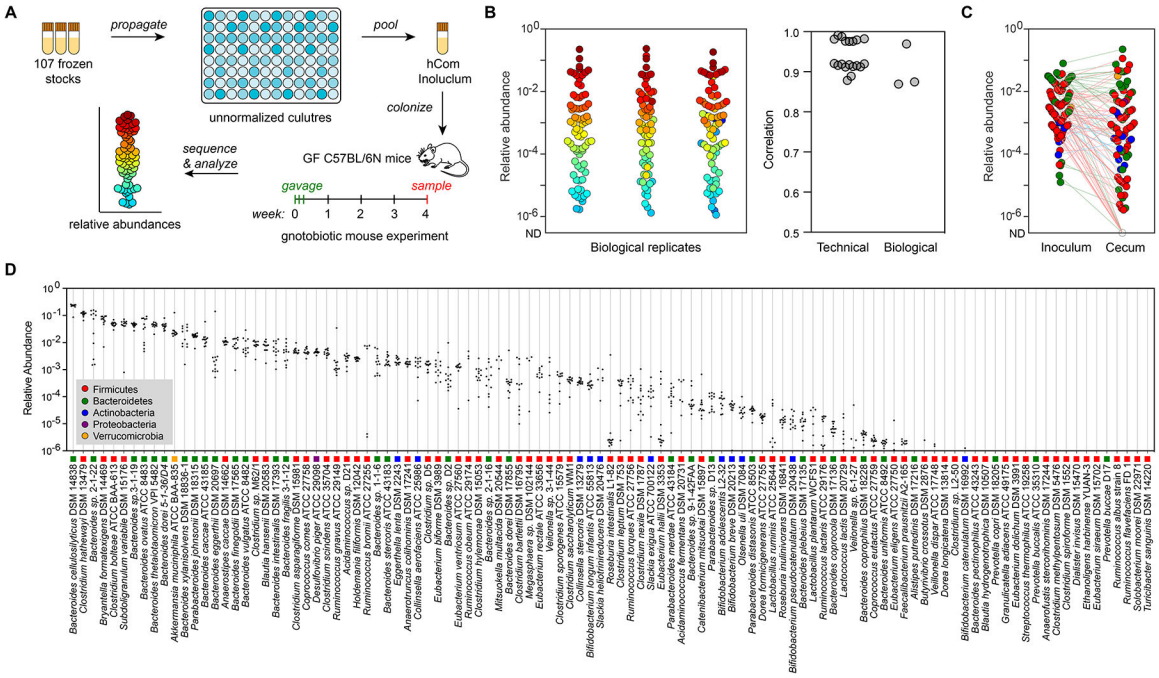

Figure 1: Colonizing germ-free C57BL/6N mice with a complex gut bacterial community (hCom1a).

(**A**) Schematic of the experiment. Frozen stocks of the 107 strains were used to inoculate cultures that were sub-cultured every 24 h and then pooled after three days. The mixed culture was used to colonize germ-free C57BL/6N mice (n=3–5 mice per replicate) by oral gavage. After four weeks of colonization, mice fed ad libitum on chow diet were sacrificed and intestinal contents were collected, subjected to metagenomic sequencing, and analyzed by NinjaMap to measure the composition of the community. (**B**) The architecture of hCom1a in the cecum is highly reproducible. Left: community composition is highly similar across three biological replicates. Each dot is an individual strain; the collection of dots in a column represents the community at 4 weeks averaged over multiple mice receiving the same inoculum. Strains are colored according to their average rank-order relative abundance across all samples. Right: Pearson's pairwise correlation coefficients for technical and biological replicates. The log10(relative abundance) values of all strains were used to calculate the Pearson correlation coefficient (R). For strains not detected, the relative abundance was set as 1e-8. (**C**) Averaged relative abundances of the inoculum versus the communities at week 4. Strains in the community span >6 orders of magnitude of relative abundance when colonizing the mouse gut. Dots are colored by phylum according to the legend in panel **D**. (**D**) Relative abundances for most strains are tightly distributed. Each column depicts the relative abundance of an individual strain across all samples at week 4. See also Figure S1 and S7, and Table S1 and S2.

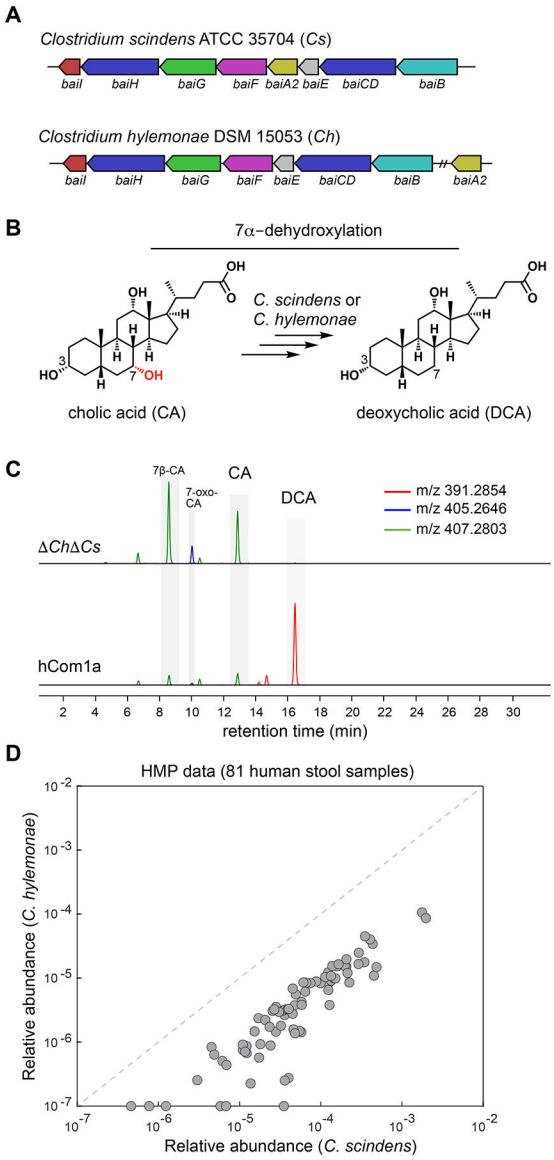

Figure 2: The 7α-dehydroxylation niche in hCom1a is composed of *Clostridium scindens* (*Cs*) and *Clostridium hylemonae* (*Ch*).

(**A**) A multigeneblast search of the 107 genomes in hCom1a shows that only *Clostridium scindens* and *Clostridium hylemonae* harbor the *bai* operon, which encodes the bile acid 7α-dehydroxylation pathway. (**B**) A simplified schematic showing the dehydroxylation of cholic acid (CA) to deoxycholic acid (DCA). (**C**) Combined extracted ion chromatogram showing that hCom1a converts CA to DCA in vitro, whereas the two-strain dropout community Δ*Ch*Δ*Cs* does not. Constituent strains were cultured separately, pooled, and subcultured (1:100) in Mega medium containing 100 μM cholic acid for 72 h. Culture supernatants were collected and analyzed by LC-MS. (**D**) *Clostridium scindens* and *Clostridium hylemonae* typically co-colonize the human gut. Each dot indicates one of the 81 gut metagenomic samples from the NIH HMP, and the relative abundance of *Cs* and *Ch* are indicated in the x axis and y-axis, respectively. See also Table S1.

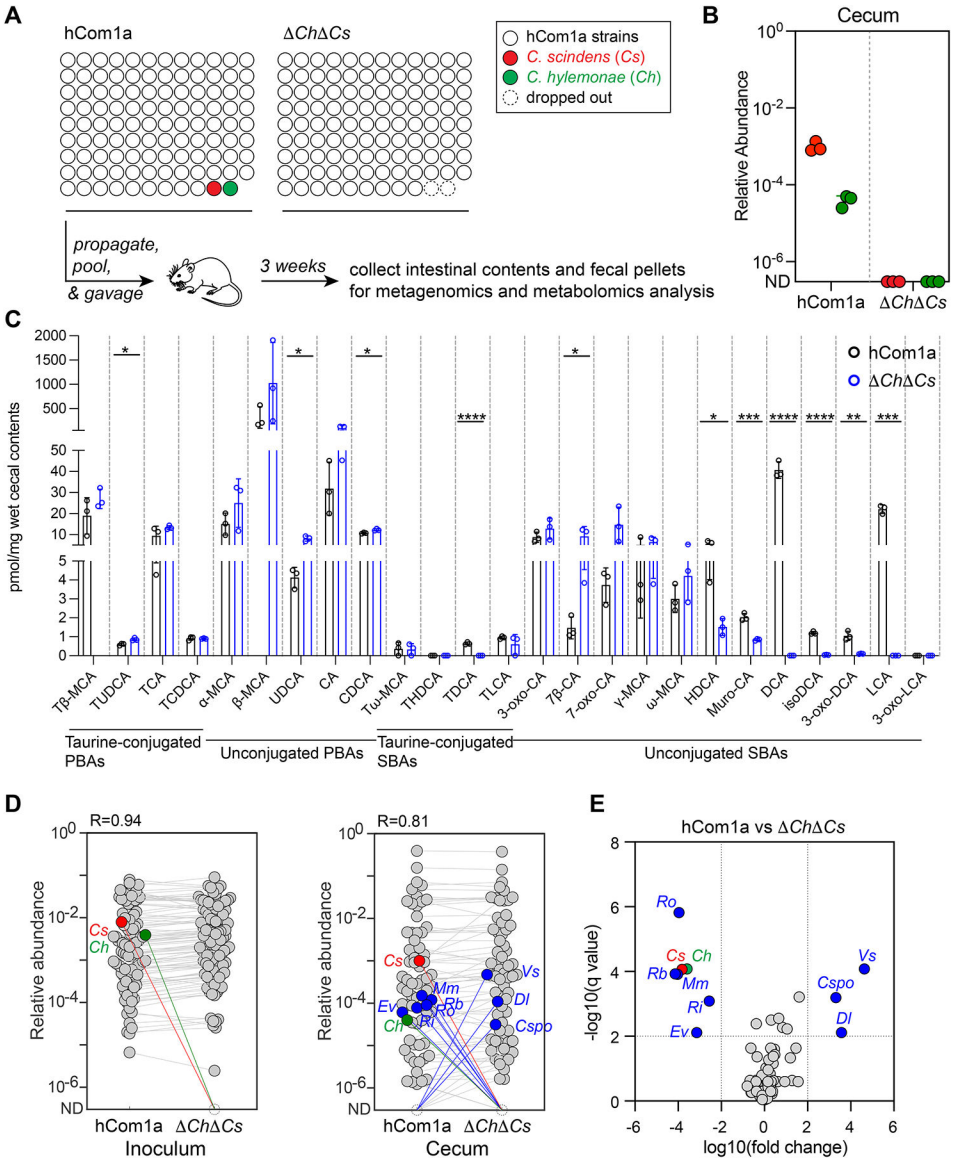

Figure 3: Metabolic and ecological impacts of removing strains in the 7α-dehydroxylation niche.

(**A**) Schematic of the experiment. Germ-free C57BL/6 mice (n=3 per group) were colonized with hCom1a or Δ*Ch*Δ*Cs* and housed for 3 weeks before sacrifice. Fecal pellets and intestinal contents were subjected to metagenomic analysis or targeted metabolite profiling. (**B**) *Cs* and *Ch* are undetectable in Δ*Ch*Δ*Cs*-colonized mice. Relative abundances were calculated through a high-resolution metagenomic analysis of the inoculum and cecal communities. (**C**) Secondary bile acids are eliminated in Δ*Ch*Δ*Cs*-colonized mice. Bile acids were quantified in cecal contents by targeted LC-MS-based profiling. Statistical significance was assessed using a Student's two-tailed t-test (*: p<0.05; **: p<0.01; ***: p<0.001; ****: p<0.0001). PBAs: primary bile acids; SBAs: secondary bile acids. (**D**) Average relative abundances of the inoculum (left) versus the cecal communities at week 3 (right). Each dot is an individual strain; the collection of dots in a column represents the community averaged over 3 mice co-housed in one cage. *Cs* and *Ch* are highlighted in red and green,

respectively. Strains highlighted in blue went up or down in relative abundance between hCom1a-colonized and Δ*Ch*Δ*Cs*-colonized mice (FDR < 0.01, fold change > 100). (**E**) Volcano plot of differential strain relative abundance. The log10(fold change) values of each strain are shown; relative abundances were set at 10^{-8} for strains not detected. Relative abundances were analyzed using a multiple unpaired t test, corrected with FDR (Q<1%). Strains discovered with significantly different relative abundance (FDR<0.01, fold change >100) are colored blue; the full names of the blue strains can be found in Figures 5D. See also Figure S2, and Table S3 and S4.

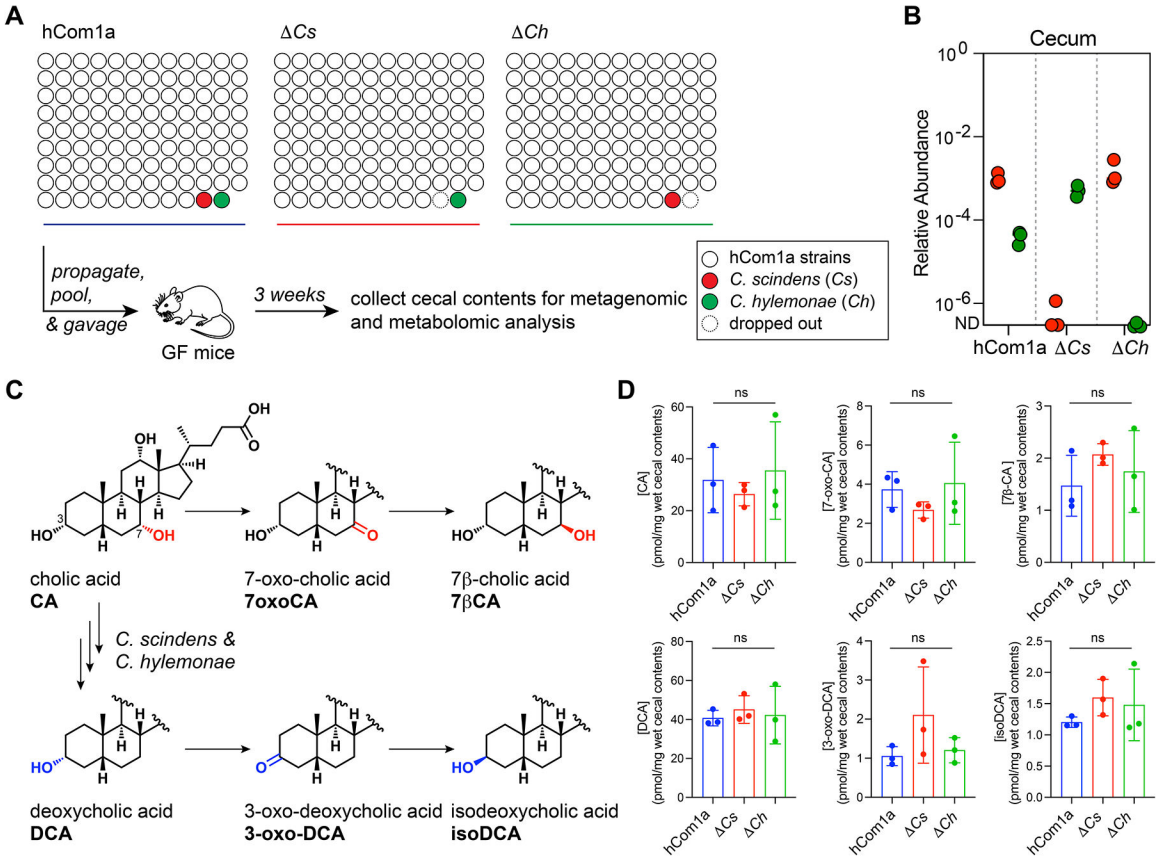

Figure 4: Compensation and functional redundancy within the 7α-dehydroxylation niche.

(**A**) Schematic of the experiment. Germ-free C57BL/6 mice (n=3 per group) were colonized with hCom1a, Δ*Cs*, or Δ*Ch* and housed for 3 weeks before sacrifice. Cecal contents were subjected to metagenomic and targeted metabolomic profiling. (**B**) Compensation within the 7α-dehydroxylation niche keeps the total relative abundance of its residents similar. Relative abundances of *Cs* and *Ch* in cecal contents from hCom1a-, Δ*Ch*-, and Δ*Cs*-colonized mice are shown. (**C**) Metabolic pathways for bile acid transformation by the gut microbiota. (**D**) The bile acid pools of mice colonized by hCom1a, Δ*Ch*, and Δ*Cs* are comparable. Thus, in the context of a complete community, *Ch* and *Cs* can carry out the core function of the niche—the conversion of primary to secondary bile acids—on its own. See also Figure S3 and S5, and Table S3 and S4.

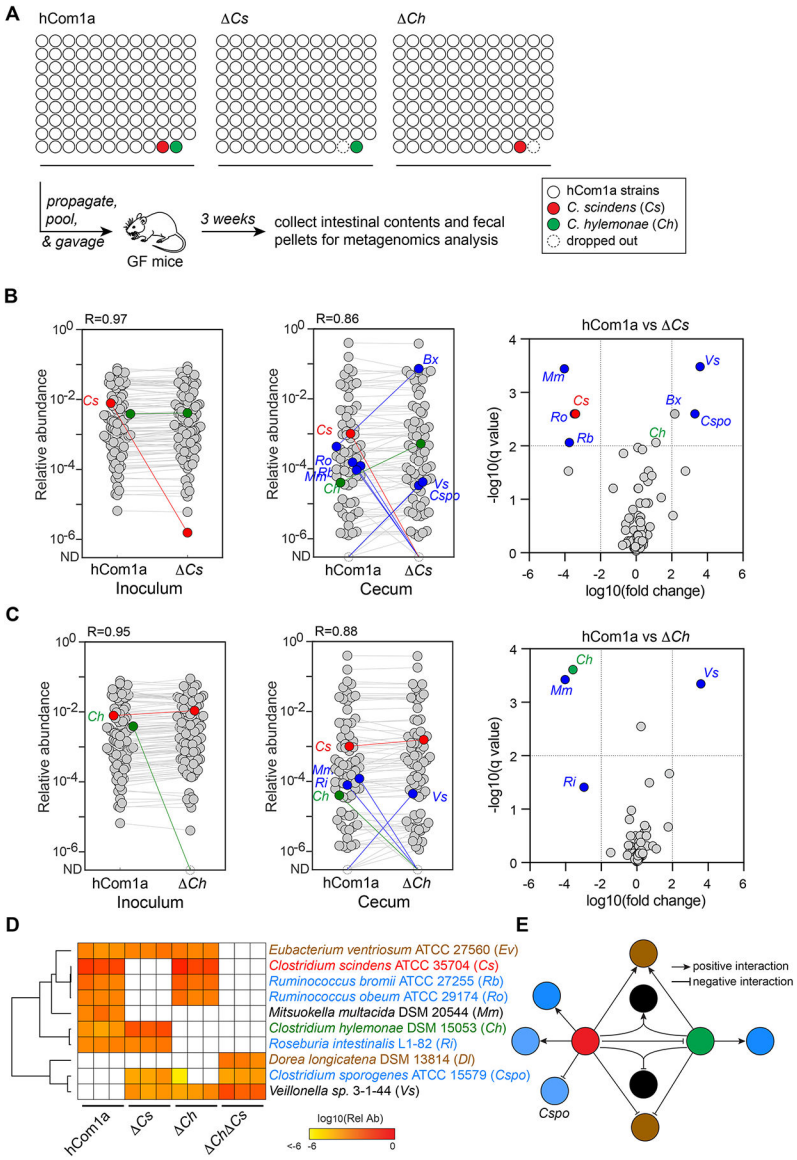

Figure 5: Single-strain dropouts reveal complex interactions among *Cs*, *Ch*, and interacting strains.

(**A**) Schematic of the experiment. Germ-free C57BL/6 mice (n=3 per group) were colonized with hCom1a, Δ*Cs*, or Δ*Ch* and housed for 3 weeks before sacrifice. Fecal pellets and intestinal contents were subjected to metagenomic analysis. (**B-C**) While most strains remain unchanged when dropping out *Cs* or *Ch*, a small number of strains change in relative abundance >100-fold. *Left:* Metagenomic analysis showing that *Cs* and *Ch* are absent in the Δ*Cs* and Δ*Ch* community inocula, respectively. *Middle:* Dropping out *Cs* or *Ch* impacts the relative abundance of five or three strains in the Δ*Cs* and Δ*Ch* communities, respectively. Each dot is an individual strain; the collection of dots in a column represents the community averaged over three mice co-housed in one cage. *Cs* and *Ch* are highlighted in red and green. Strains colored blue went up or down in relative abundance between hCom1a-colonized and Δ*Cs* or Δ*Ch*-colonized mice (FDR<0.01, fold change >100). *Right:* Volcano plot showing the log10(fold change) values for each strain; for strains that were not detected, relative

abundances were set at 10^{-8}. Strains with significantly different relative abundance (FDR <0.01, fold change $>10^2$) are colored blue; the full names of these strains are shown next to the heatmap in (**D**). The change in the relative abundance of *Bacteroides xylanisolvens* DSM 18836 (*Bx*) was close to the cutoff in Δ*Cs* but not the other communities; this strain is not further discussed. (**D**) Heatmap representing the 8-strain interaction network around *Cs* and *Ch*. The relative abundance of each strain is shown in three mice colonized by hCom1a, Δ*Cs*, Δ*Ch*, or Δ*Ch*Δ*Cs*. Strains with relative abundance $<10^{-6}$ are colored white. (**E**) Schematic of the interaction network. Strains are linked to the 7α-dehydroxylation niche in one of three ways: 1) Some strains are specific to *Cs* (*Rb, Ro*, and *Cspo*) or *Ch* (*Ri*); these interactions are presumably strain-specific and unrelated to bile acids. 2) *Ev* and *Dl* only respond to the double-strain dropout, indicating a mechanism related to secondary bile acid production. 3) The remaining strains, *Mm* and *Vs*, respond when either or both strains are missing, suggesting a requirement for the simultaneous presence of *Cs* and *Ch*. See also Figure S2 and S5, and Table S3.

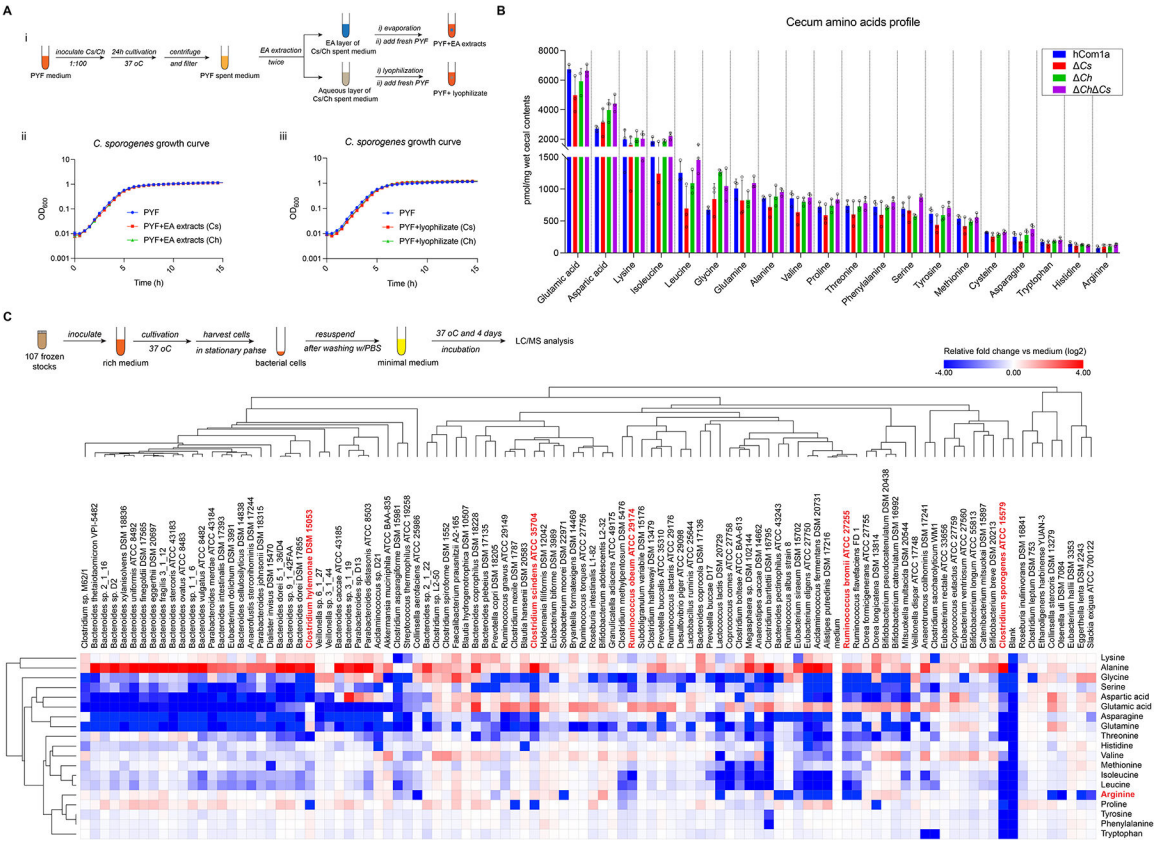

Figure 6: Investigating the mechanism of the interaction between *Cs* and *Cspo*.

(**A**) No diffusible antimicrobial metabolites are found in the culture fluid of *C. scindens* (*Cs*) or *C. hylemonae* (*Ch*). (**i**) Schematic of preparing EA extracts and lyophilizate from the spent medium of *Cs* and *Ch* cultures. (**ii**) Growth curves of *Cspo* in fresh PYF medium without or with the EA extracts or lyophilizate from the spent medium of *Cs* or *Ch*. (**B**) Targeted profiling of amino acids in the cecum of hCom1a-, Δ*Cs*-, Δ*Ch*- and Δ*Ch*Δ*Cs*- colonized mice by LC-MS. (**C**) Targeted profiling of amino acid depletion by hCom1a strains *in vitro*. (Top) schematic of the experiment. (Bottom) heatmap of amino acid depletion by hCom1a strains, clustered by one minus pearson correlation. The abundance of each amino acid was normalized to the bacteria-free control (medium); in the log2 transformed data, red indicates an increased concentration while blue means the concentration has decrease. The data represent one of two independent experiments. See also Figure S6.

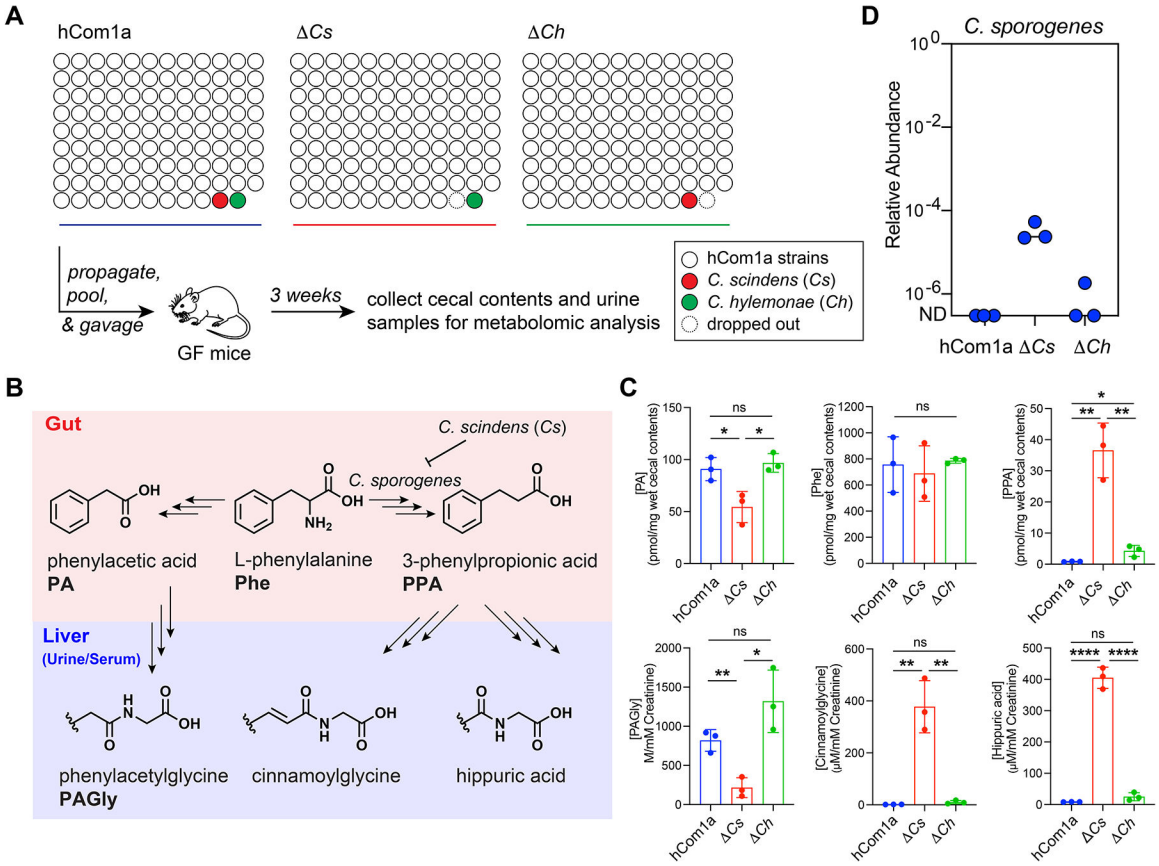

Figure 7: An unexpected impact of *Cs* on aromatic amino acid metabolism.

(**A**) Schematic of the experiment. Germ-free C57BL/6 mice (n=3 per group) were colonized with hCom1a or its single-strain dropout variant (Δ*Cs* and Δ*Ch*) and housed for 3 weeks before sacrifice. Fecal pellets, cecal contents, and urine samples were subjected to targeted metabolite profiling. (**B**) Certain gut bacteria can reduce phenylalanine (Phe) to phenylpropionic acid (PPA), which is converted to hippuric acid and cinnamoylglycine by the host. Other gut bacteria oxidize Phe to phenylacetic acid (PA), which is metabolized in the liver to phenylacetylglycine (PAGly). (**C**) Δ*Cs* differs markedly from hCom1a and Δ*Ch* in terms of AAA metabolite output. hCom1a and Δ*Ch* convert phenylalanine almost exclusively to PA (from which the host generates PAGly); hippurate is nearly undetectable in the urine and serum (Figure S3). In contrast, Δ*Cs* converts Phe predominantly to phenylpropionic acid (which the host metabolizes to hippurate); PAGly levels are very low in the urine and serum (Figure S3). (**D**) *C. sporogenes*, which is undetectable in hCom1a- and Δ*Ch*-colonized mice, rises to a relative abundance of 10^{-5}-10^{-4} in Δ*Cs*-colonized mice. The relative abundance of *Cspo* in cecal contents from hCom1a-, Δ*Cs*-, and Δ*Ch*-colonized mice is shown. Statistical significance was assessed using a Student's two tailed t-test (*: p<0.05; **: p<0.01; ***: p<0.001; ****: p<0.0001, n.s: no significance). See also Figure S2, S3, and S5, and Table S4.

KEY RESOURCES TABLE

REAGENT or RESOURCE	SOURCE	IDENTIFIER
Bacterial and Virus Strains		
Alistipes putredinis DSM 17216	DSMZ	Chopped Meat Medium
Anaerotruncus colihominis DSM 17241	DSMZ	Mega Medium
Bacteroides caccae ATCC 43185	ATCC	Mega Medium
Bacteroides coprophilus DSM 18228	DSMZ	Mega Medium
Bacteroides dorei 5_1_36/D4	BEI	Mega Medium
Bacteroides eggerthii DSM 20697	DSMZ	Mega Medium
Bacteroides finegoldii DSM 17565	DSMZ	Mega Medium
Bacteroides fragilis 3_1_12	BEI	Mega Medium
Bacteroides intestinalis DSM 17393	DSMZ	Mega Medium
Bacteroides sp. 1_1_6	BEI	Mega Medium
Bacteroides sp. 2_1_22	BEI	Mega Medium
Bacteroides sp. 3_1_19	BEI	Mega Medium
Bacteroides sp. 9_1_42FAA	BEI	Mega Medium
Bacteroides sp. 2_1_16	BEI	Mega Medium
Bacteroides sp. D2	BEI	Mega Medium
Bacteroides thetaiotaomicron VPI-5482	ATCC	Mega Medium
Bacteroides xylanisolvens DSMZ 18836	DSMZ	Mega Medium
Bacteroides uniformis ATCC 8492	ATCC	Mega Medium
Bacteroides pectinophilus ATCC 43243	ATCC	Chopped Meat Medium
Bacteroides plebeius DSM 17135	DSMZ	Chopped Meat Medium
Bacteroides coprocola DSM 17136	DSMZ	Chopped Meat Medium
Bacteroides stercoris ATCC 43183	DSMZ	Mega Medium
Coprococcus eutactus ATCC 27759	ATCC	Chopped Meat Medium
Eubacterium dolichum DSM 3991	DSMZ	Mega Medium
Ruminococcus gnavus ATCC 29149	BEI	Mega Medium
Eubacterium rectale ATCC 33656	ATCC	Mega Medium
Clostridium methylpentosum DSM 5476	DSMZ	Mega Medium
Clostridium nexile DSM 1787	DSMZ	Mega Medium
Clostridium scindens ATCC 35704	ATCC	Mega Medium
Clostridium sp. L2–50	BEI	Chopped Meat Medium
Clostridium sp. M62/1	BEI	Chopped Meat Medium
Clostridium asparagiforme DSM 15981	DSMZ	Mega Medium
Clostridium bolteae ATCC BAA-613	ATCC	Mega Medium
Clostridium hathewayi DSM 13479	DSMZ	Mega Medium
Clostridium leptum DSM 753	DSMZ	Chopped Meat Medium
Dorea formicigenerans ATCC 27755	DSMZ	Mega Medium

REAGENT or RESOURCE	SOURCE	IDENTIFIER
Dorea longicatena DSM 13814	DSMZ	Mega Medium
Coprococcus comes ATCC 27758	ATCC	Mega Medium
Blautia hansenii DSM 20583	DSMZ	Mega Medium
Bryantella formatexigens DSM 14469	DSMZ	Mega Medium
Butyrivibrio crossotus DSM 2876	DSMZ	Chopped Meat Medium
Ruminococcus torques ATCC 27756	ATCC	Mega Medium
Parabacteroides merdae ATCC 43184	DSMZ	Mega Medium
Subdoligranulum variabile DSM 15176	DSMZ	Mega Medium
Parabacteroides johnsonii DSM 18315	DSMZ	Chopped Meat Medium
Roseburia intestinalis L1–82	ATCC	Mega Medium
Ruminococcus obeum ATCC 29174	DSMZ	Mega Medium
Eubacterium ventriosum ATCC 27560	DSMZ	Mega Medium
Faecalibacterium prausnitzii A2–165	DSMZ	Chopped Meat Medium
Parabacteroides sp. D13	BEI	Mega Medium
Eubacterium hallii DSM 3353	DSMZ	Chopped Meat Medium
Roseburia inulinivorans DSM 16841	DSMZ	Chopped Meat Medium
Prevotella buccalis ATCC 35310	DSMZ	Chopped Meat Medium
Ruminococcus lactaris ATCC 29176	ATCC	Chopped Meat Medium
Eubacterium eligens ATCC 27750	DSMZ	Mega Medium
Holdemania filiformis DSM 12042	DSMZ	Mega Medium
Bacteroides ovatus ATCC 8483	ATCC	Mega Medium
Bacteroides vulgatus ATCC 8482	ATCC	Mega Medium
Clostridium spiroforme DSM 1552	DSMZ	Chopped Meat Medium
Eubacterium biforme DSM 3989	DSMZ	Mega Medium
Blautia hydrogenotrophica DSM 10507	DSMZ	Chopped Meat Medium
Clostridium saccharolyticum WM1	DSMZ	Mega Medium
Parabacteroides distasonis ATCC 8503	ATCC	Mega Medium
Eubacterium siraeum DSM 15702	DSMZ	Chopped Meat Medium
Eggerthella lenta DSM 2243	DSMZ	Chopped Meat Medium
Anaerostipes caccae DSM 14662	DSMZ	Mega Medium
Bacteroides cellulosilyticus DSM 14838	DSMZ	Mega Medium
Clostridium hylemonae DSM 15053	DSMZ	Mega Medium
Acidaminococcus sp. D21	BEI	Mega Medium
Catenibacterium mitsuokai DSM 15897	DSMZ	Mega Medium
Collinsella aerofaciens ATCC 25986	ATCC	Mega Medium
Acidaminococcus fermentans DSM 20731	DSMZ	Mega Medium
Clostridium bartlettii DSM 16795	DSMZ	Mega Medium
Ethanoligenens harbinense YUAN-3	DSMZ	Chopped Meat Medium
Veillonella dispar ATCC 17748	DSMZ	Chopped Meat Medium

REAGENT or RESOURCE	SOURCE	IDENTIFIER
Collinsella stercoris DSM 13279	DSMZ	Chopped Meat Medium
Prevotella buccae D17	BEI	Chopped Meat Medium
Mitsuokella multacida DSM 20544	DSMZ	Mega Medium
Olsenella uli DSM 7084	DSMZ	Chopped Meat Medium
Slackia heliotrinireducens DSM 20476	DSMZ	Chopped Meat Medium
Bifidobacterium longum infantis ATCC 55813	BEI	Mega Medium
Dialister invisus DSM 15470	DSMZ	Mega Medium
Prevotella copri DSM 18205	DSMZ	Chopped Meat Medium
Veillonella sp. 6_1_27	BEI	Chopped Meat Medium
Slackia exigua ATCC 700122	DSMZ	Chopped Meat Medium
Streptococcus thermophilus LMD-9	ATCC	Chopped Meat Medium
Desulfovibrio piger ATCC 29098	DSMZ	Chopped Meat Medium
Lactobacillus ruminis ATCC 25644	ATCC	Mega Medium
Akkermansia muciniphila ATCC BAA-835	DSMZ	Mega Medium
Bifidobacterium adolescentis L2–32	BEI	Mega Medium
Bifidobacterium pseudocatenulatum DSM 20438	DSMZ	Mega Medium
Solobacterium moorei DSM 22971	DSMZ	Chopped Meat Medium
Anaerofustis stercorihominis DSM 17244	DSMZ	Mega Medium
Lactococcus lactis DSMZ 20729	DSMZ	Mega Medium
Granulicatella adiacens ATCC 49175	DSMZ	Mega Medium
Clostridium sporogenes ATCC 15579	ATCC	Mega Medium
Bacteroides dorei DSM 17855	DSMZ	Mega Medium
Bifidobacterium catenulatum DSM 16992	DSMZ	Mega Medium
Ruminococcus albus strain 8	Laboratory of Robert Mackie	Chopped Meat Medium
Ruminococcus flavefaciens FD 1	Laboratory of Robert Mackie	Chopped Meat Medium
Ruminococcus bromii ATCC (L2–63)	ATCC	Chopped Meat Medium
Veillonella sp. 3_1_44	BEI	Chopped Meat Medium
Bifidobacterium breve DSM 20213	DSMZ	Mega Medium
Megasphaera sp. DSMZ 102144	DSMZ	Mega Medium
Clostridium sp. D5	BEI	Mega Medium
Lactobacillus plantarum WCFS1	ATCC	Mega Medium
Turicibacter sanguinis DSM 14220	DSMZ	Chopped Meat Medium
Paenibacillus barengoltzii CC33–002B	BEI	Mega Medium
Chemicals, Peptides, and Recombinant Proteins		
PBS	Gibco	10010023
Tryptone peptone	Difco	211921

REAGENT or RESOURCE	SOURCE	IDENTIFIER
Bacto yeast extract	Difco	212750
Magnesium sulfate heptahydrate	Sigma	M2773
Sodium bicarbonate	Sigma	S5761
Calcium chloride	Sigma	C7902
Resazurin	Sigma	R7017
Agar	Difco	DF0140-01-0
Sodium acetate	Sigma	S2889
Meat extract	Sigma	70164
D-glucose	Sigma	47829
L-cystine HCl	Sigma	C7477
Potassium phosphate monobasic	Sigma	P5655
Potassium phosphate dibasic	Sigma	P3786
Vitamin K3	Sigma	M5625
Hematin	Sigma	H3281
Tween 80	Sigma	P4780
Vitamin mix	ATCC	MD-VS
Trace mineral supplement	ATCC	MD-TMS
D-(+)-cellobiose	Sigma	C7252
D-(+)-maltose monohydrate	Sigma	M5885
D-(−)-fructose	Sigma	F0127
Acetic acid, glacial	Sigma	A6283
Propionic acid	Sigma	P5561
Butyric acid	Sigma	B103500
Isovaleric acid	Sigma	129542
Sterilized rumen fluid	Bar Diamond Ranch	#SRF
Chopped meat media	Hardy Diagnostics	K219
Vitamin K2	Sigma	V9378
Ammonium sulfate	Sigma	A4418
Nitrilotriacetic acid	Sigma	N9877
Manganese(II) chloride tetrahydrate	Sigma	M5005
Cobalt (II) hexahydrate	Sigma	C8661
Calcium chloride dihydrate	Sigma	223506
Zinc chloride	Sigma	Z0152
Copper chloride	Sigma	451665
Sodium molybdate dihydrate	Sigma	M1651
Boric acid	Sigma	B6768
Sodium selenite	Sigma	214485

REAGENT or RESOURCE	SOURCE	IDENTIFIER
Nickel chloride hexahydrate	Sigma	N6136
Sodium tungstate dihydrate	Sigma	72069
L-alanine	Sigma	A7469
L-arginine	Sigma	A5006
L-asparagine	Sigma	A4159
L-aspartic Acid	Sigma	A8949
L-glutamic Acid	Sigma	49449
L-glutamine	Sigma	49419
L-glycine	Sigma	G7126
L-histidine	Fisher	BP382
L-isoleucine	TCI	I0181
L-leucine	TCI	L0029
L-lysine	Sigma	L5751
L-methionine	Sigma	64319
L-phenylalanine	Sigma	P5482
L-proline	Sigma	81709
L-serine	Sigma	S4500
L-threonine	Sigma	89179
L-tryptophan	Sigma	T0254
L-tyrosine	Sigma	93829
L-valine	Sigma	94619
Columbia agar with 5% sheep blood	BD	221165
Brain Heart Infusion broth	Fisher	CM1136B
Horse blood, defibrinated	Fisher	50863761
Peptone Yeast Extract Broth with Fructose	Anaerobe Systems	AS-840
Glycerol	Fisher	PRH5433
Potassium chloride	Sigma	P9541
Magnesium chloride	Sigma	M1028
Sodium phosphate dibasic	Sigma	S3264
Sodium chloride	Sigma	S3014
Methanol	Fisher	A456
Formic acid	Sigma	426229
Ammonium bicarbonate	Sigma	9830
Ammonium formate	Sigma	70221
Acetonitrile	Fisher	A955
4-chloro-L-phenylalanine	Carbosynth	FC13398
Taurobetamuricholic acid	Steraloids	C1899–000
Tauroursodeoxycholic acid	Sigma	580549

REAGENT or RESOURCE	SOURCE	IDENTIFIER
Taurocholic acid	Sigma	86339
Taurochenodeoxycholate	Sigma	T6260
Alphamuricholic acid	Steraloids	C1890–000
Betamuricholic acid	Steraloids	C1895–000
Ursodeoxycholic acid	Sigma	U5127
Cholic acid	Sigma	C1129
Chenodeoxycholic acid	Sigma	c9377
Tauroomegamuricholic acid	Steraloids	C1889–000
Taurohyodeoxycholic acid	Steraloids	C0890–000
Taurodeoxycholic acid	Sigma	T0557
Taurolithocholic acid	Sigma	T7515
3-oxocholic acid	Steraloids	C1272–000
7-betacholic acid	TRC	U849900
7-oxocholic acid	Sigma	SMB00806
Gammamuricholic acid	Steraloids	C1850–000
Omegamuricholic acid	Steraloids	C1888–000
Hyodeoxycholic acid	Sigma	H3878
Murocholic acid	Steraloids	C0910–000
Deoxycholic acid	Sigma	D2510
Isodeoxycholic acid	Steraloids	C1165–000
3-oxodeoxycholic Acid	TRC	O856870
Lithocholic acid	Sigma	L6250
3-oxolithocholic acid	TRC	O848490
Cholic acid-2,2,4,4-d4	Sigma	614149
1-acetyl-β-carboline	Aobious	CFN92122
Critical Commercial Assays		
DNeasy Power Soil Kit	Qiagen	12955–4
Illumina NextSeq Kit	Illumina	NextSeq 500/550 v2.5
Illumina NovaSeq kit	Illumina	NovaSeq 6000 S4 Reagent Kit v1.5
Pico488 dsDNA quantification reagent	Lumiprobe	92010
Creatinine Assay Kit	Abcam	ab204537
Deposited Data		
Raw metabolomics data	This study	MassIVE (ftp://massive.ucsd.edu/MSV000091763/)
Experimental Models: Organisms/Strains		
Mouse: C57BL/6 GF	Taconic Biosciences	N/A

REAGENT or RESOURCE	SOURCE	IDENTIFIER
Mouse: Swiss-Webster GF	Taconic Biosciences	N/A
Software and Algorithms		
NinjaMap	Cheng et al.[16]	https://github.com/FischbachLab/ninjaMap/releases/tag/cheng_et_al
Bowtie2 v. 2.3.5.1	Langmead et al.[39]	https://bowtie-bio.sourceforge.net/bowtie2/index.shtml
Matlab R2022a	MathWorks	https://www.mathworks.com/products/matlab.html
Prism v. 9.3.1	GraphPad software	https://www.graphpad.com/features
Morpheus	N/A	https://software.broadinstitute.org/morpheus
MassHunter Qualitative Analysis Software v. 7.0	Agilent	https://www.agilent.com/en/product/software-informatics/mass-spectrometry-software/data-analysis/qualitative-analysis
MassHunter Quantitative Analysis Software v. B.09.00	Agilent	https://www.agilent.com/en/product/software-informatics/mass-spectrometry-software/data-analysis/quantitative-analysis
Other		
Precellys® CK28 Hard Tissue Homogenizing Kit, Beads	VWR	10144–494
Durapore PVDF 0.22-μm membrane	Millipore	UFC30GV00
MultiScreen Solvinert 96 Well Filter Plate	Millipore	MSRLN0410
1.2 ml V-bottom 96-well plates	Thomas Scientific	OX1263-S
2.2 ml V-bottom 96-well deep-well plates	Thomas Scientific	OX1265-S
Silicone fitted plate mat	Thomas Scientific	EK-2066
Corning 96 Well Clear Flat Bottom, Polystyrene, sterile	Corning	3370
Vinyl Tape	Coy	1600330w
Microplate spectrophotometer	BioTeK	Epoch2
Tissue Lyser II	Qiagen	N/A
ACQUITY UPLC BEH C18 Column, 130Å, 1.7 μm, 2.1 mm×100 mm	Waters	186002352
ACQUITY UPLC BEH C18 VanGuard Pre-column, 130 Å, 1.7 μm, 2.1	Waters	186003975

REAGENT or RESOURCE	SOURCE	IDENTIFIER
ACQUITY UPLC BEH Amide VanGuard Pre-column, 130 Å, 1.7 μm, 2.1	Waters	186004799
Waters ACQUITY UPLC BEH Amide Column, 130Å, 1.7 μm, 2.1 mm×150 mm	Waters	186004802
Kinetex C18 column (1.7 μm, 2.1×100 mm)	Phenomenex	N/A
Agilent 1290 Infinity II UPLC	Agilent	N/A
Agilent 6530 QTOF MS	Agilent	N/A